

Sensing and signaling of oxidative stress in chloroplasts by inactivation of the SAL1 phosphoadenosine phosphatase

Chan, Kai Xun; Mabbitt, Peter; Phua, Su Yin ; Mueller, Jonathan Wolf; Nisar, Nazia ; Gigolashvili, Tamara; Stroehrer, Elke; Grassl, Julia; Arlt, Wiebke; Estavillo, Gonzalo; Jackson, Colin; Pogson, Barry

DOI:

[10.1073/pnas.1604936113](https://doi.org/10.1073/pnas.1604936113)

License:

None: All rights reserved

Document Version

Peer reviewed version

Citation for published version (Harvard):

Chan, KX, Mabbitt, P, Phua, SY, Mueller, JW, Nisar, N, Gigolashvili, T, Stroehrer, E, Grassl, J, Arlt, W, Estavillo, G, Jackson, C & Pogson, B 2016, 'Sensing and signaling of oxidative stress in chloroplasts by inactivation of the SAL1 phosphoadenosine phosphatase', *National Academy of Sciences. Proceedings*, vol. 113, no. 31, pp. E4567-E4576. <https://doi.org/10.1073/pnas.1604936113>

[Link to publication on Research at Birmingham portal](#)

Publisher Rights Statement:

Eligibility for repository: Checked on 10/6/2016

General rights

Unless a licence is specified above, all rights (including copyright and moral rights) in this document are retained by the authors and/or the copyright holders. The express permission of the copyright holder must be obtained for any use of this material other than for purposes permitted by law.

- Users may freely distribute the URL that is used to identify this publication.
- Users may download and/or print one copy of the publication from the University of Birmingham research portal for the purpose of private study or non-commercial research.
- User may use extracts from the document in line with the concept of 'fair dealing' under the Copyright, Designs and Patents Act 1988 (?)
- Users may not further distribute the material nor use it for the purposes of commercial gain.

Where a licence is displayed above, please note the terms and conditions of the licence govern your use of this document.

When citing, please reference the published version.

Take down policy

While the University of Birmingham exercises care and attention in making items available there are rare occasions when an item has been uploaded in error or has been deemed to be commercially or otherwise sensitive.

If you believe that this is the case for this document, please contact UBIRA@lists.bham.ac.uk providing details and we will remove access to the work immediately and investigate.

2
3 **Sensing and signaling of oxidative stress in chloroplasts by inactivation of the SAL1**
4 **phosphoadenosine phosphatase**

5 *Short title: Sensing of chloroplast oxidative stress by SAL1*
6

7 Kai Xun Chan^a, Peter D. Mabbitt^b, Su Yin Phua^a, Jonathan W. Mueller^c, Nazia Nisar^a, Tamara
8 Gigolashvili^d, Elke Stroeher^e, Julia Grassl^e, Wiebke Arlt^c, Gonzalo M. Estavillo^{a,1}, Colin J.
9 Jackson^b, Barry J. Pogson^{a,2}.

10 ^aARC Centre of Excellence in Plant Energy Biology, Research School of Biology, Australian
11 National University, Acton ACT 2601, Australia

12 ^bResearch School of Chemistry, Australian National University, Acton ACT 2601, Australia

13 ^cInstitute of Metabolism and Systems Research (IMSR), University of Birmingham & Centre for
14 Endocrinology, Diabetes and Metabolism (CEDAM), Birmingham Health Partners, Birmingham,
15 B15 2TT, UK

16 ^dBotanical Institute and Cluster of Excellence on Plant Sciences (CEPLAS), University of
17 Cologne, 50674 Cologne, Germany

18 ^eARC Centre of Excellence in Plant Energy Biology, University of Western Australia, Crawley
19 WA 6009, Australia

20 ¹Current Address: CSIRO Agriculture, Black Mountain, Canberra, Australia.

21 ²**Corresponding author:** Barry J. Pogson (+61 2 61255629; barry.pogson@anu.edu.au)
22

23 **Keywords:** Retrograde signaling, redox regulation, stress sensing
24

Abstract

Intracellular signaling during oxidative stress is complex, with organelle-to-nucleus retrograde communication pathways ill-defined or incomplete. Here we identify the 3'-phosphoadenosine 5'-phosphate (PAP) phosphatase SAL1 as a novel and conserved oxidative stress sensor in plant chloroplasts. *Arabidopsis thaliana* SAL1 (AtSAL1) senses changes in photosynthetic redox poise, hydrogen peroxide, and superoxide concentrations in chloroplasts *via* redox regulatory mechanisms. AtSAL1 phosphatase activity is suppressed by dimerization, intramolecular disulfide formation and glutathionylation, allowing accumulation of its substrate, PAP; a chloroplast stress retrograde signal that regulates expression of Plastid Redox Associated Nuclear Genes (PRANGs). This redox regulation of SAL1 for activation of chloroplast signaling is conserved in the plant kingdom, and the plant protein has evolved enhanced redox sensitivity compared to its yeast ortholog. Our results indicate that, in addition to sulfur metabolism, SAL1 orthologs have evolved secondary functions in oxidative stress sensing in the plant kingdom.

Significance Statement

Management of oxidative stress in plant chloroplasts involves signaling pathways to the nucleus that trigger stress response mechanisms. Yet, how oxidative stress is initially sensed in the chloroplast to activate accumulation of a stress signal remains enigmatic. We show that inactivation of a phosphatase, SAL1, by oxidative stress in chloroplasts controls accumulation of its substrate, as a plant stress signal. This regulatory mechanism is highly conserved across the plant kingdom and confers a second function to this metabolic enzyme as an oxidative stress sensor.

1 Introduction

2 Alleviating oxidative stress is a common challenge across evolution, occurring at the cellular,
3 organellar and systemic levels. In plant chloroplasts, drought and high light (HL) stress induce
4 production of reactive oxygen species (ROS) such as singlet oxygen ($^1\text{O}_2$) at Photosystem II
5 (PSII), and hydrogen peroxide (H_2O_2) as well as superoxide (O_2^-) at Photosystem I (PSI) (1).
6 There is also a shift from reducing to more oxidizing states in the redox poise of plastoquinone
7 (PQ) and other stromal redox couples such as glutathione (GSH/GSSG). All of these changes are
8 associated with adjustment of photosystem stoichiometry and chloroplastic metabolic enzymes
9 by chloroplast-resident kinases (2) and redox-sensitive thioredoxins (3) respectively; as well as
10 activation of signaling pathways for the induction of common and unique sets of nuclear genes
11 (4, 5).

12 The nuclear transcriptional response to stress in chloroplasts is mediated by chemical signals
13 emanating from the chloroplasts to the nucleus in a process called retrograde signaling (6). There
14 are at least seven distinct retrograde signaling pathways responding to changes in chloroplastic
15 ROS and redox state (7); including beta-cyclocitral for PSII- $^1\text{O}_2$ responses (8) and PAP-XRN
16 pathway which alters expression of 25% of the HL-associated transcriptome, many of which are
17 ROS and redox associated (9). The unique gene sets which expression are induced by PSI ROS
18 and changes in chloroplast redox poise are collectively referred to herein as PRANGs (Plastid
19 Redox Associated Nuclear Genes) (7); they include key and common stress marker genes such as
20 *ASCORBATE PEROXIDASE 2 (APX2)* (10, 11) and *ZAT10* (12) critical for acclimation. The
21 nuclear regulators of PRANGs and the subsequent chloroplast-targeted stress responses,
22 including induction of chloroplast antioxidant and redox regulation enzymes such as redoxin
23 proteins, have been extensively elucidated for the different retrograde pathways (7, 12). Despite

these advances, however, in all of the PRANG retrograde signaling pathways no chloroplastic sensor(s) of ROS and redox state has been conclusively identified (7). For instance, a previously hypothesized sensor kinase for the PQ redox state (2) has recently been re-ascribed to facilitate H₂O₂ production rather than redox sensing *per se* (13).

A substantial proportion of PRANGs are regulated by the phosphonucleotide, 3'-phosphoadenosine 5'-phosphate (PAP), which acts as a mobile chloroplast-to-nucleus stress retrograde signal (9). PAP accumulation is induced by drought and high-light stress, and the metabolite signal moves between the chloroplast, cytosol and nucleus (9). PAP is produced by sulfotransferase-catalyzed sulfation reactions in secondary sulfur metabolism, which transfer activated sulfate from 3'-phosphoadenosine 5'-phosphosulfate (PAPS) to various key acceptor molecules including peptides and hormones (14). This sulfate transfer generates PAP as a by-product that inhibits sulfotransferase activity and feedback-regulates overall sulfur flux (14, 15). During unstressed conditions, PAP is enzymatically degraded by the *Arabidopsis thaliana* SAL1 (AtSAL1) phosphatase in the chloroplast (9). AtSAL1 loss-of-function leads to constitutive PAP accumulation, up-regulation of PRANGs, increased stress tolerance and altered sulfur metabolism (9, 15). Hence, SAL1 and PAP perform dual functions in sulfur metabolism (15) and stress signaling (9). The role of SAL1-PAP in chloroplast stress signaling is likely conserved beyond *Arabidopsis* to other members of the plant kingdom, since transient silencing of SAL1 also enhanced stress tolerance in wheat (*Triticum aestivum*) (16).

PAP controlling PRANG expression during drought and HL has known degradation and production site(s) for the signal, a mechanism for signal movement, and a protein target for the signal (7, 9). Yet, similar to all other PRANG-regulating retrograde pathways, the mechanism by which chloroplast oxidative stress and redox state are initially sensed and transduced is

unknown. Here we demonstrate that contrary to expectation for a metabolic enzyme, SAL1 can in and of itself act as a molecular sensor for oxidative stress. The switches for accumulation of the PAP chloroplast retrograde signal reside within the SAL1 protein, thereby providing a common site of perception of PSI ROS and redox couples for regulating PRANGs.

Results

Accumulation of the stress signal PAP occurs *via* oxidative down-regulation of AtSAL1 activity

Given the multiple redox couples altered in the chloroplast in response to HL and drought (1, 14), we hypothesized that PAP accumulation during these stress conditions (9) can be regulated by AtSAL1 if the enzyme acted as a sensor of, and its activity regulated by, oxidative stress. Indeed, PSI-sourced ROS that invoke PRANG regulation such as H_2O_2 and O_2^- significantly lowered *in vivo* AtSAL1 activity (**Fig. 1A**). This was replicated in plants exposed to the abiotic stresses drought and HL that induce H_2O_2 and O_2^- formation (**Fig. 1A**). These treatments did not significantly alter AtSAL1 protein abundance however (**Fig. 1A**), suggesting that the regulation of AtSAL1 activity in the chloroplast is therefore most likely *via* a post-translational mechanism(s).

It is well established that in mutants deficient in regeneration of oxidized proteins, redox buffer homeostasis (NADPH/NADP^+ , GSH/GSSG), or the water-water cycle that degrades PSI O_2^- and H_2O_2 *via* ascorbate (1); there is increased ROS accumulation, shifts in redox balance towards more oxidizing states, and /or deregulated PRANG expression (see **Table S1**). In six of such mutants, *in vivo* AtSAL1 activity in response to HL-induced oxidative stress was further reduced by up to 50% relative to wild type (WT) (**Fig. 1B**).

AtSAL1 is redox-regulated by dual mechanisms of intramolecular disulfide formation and dimerization

The suppression of *in vivo* AtSAL1 activity under oxidative stress conditions (**Fig. 1A**), co-regulation of PRANG expression by photosynthetic ROS and PAP (4, 5, 9), and redox regulation of some sulfur metabolism enzymes in chloroplasts (14), led us to hypothesize that down-regulation of *in vivo* AtSAL1 activity is directly mediated by redox potential. Indeed, *in vitro* AtSAL1 activity is decreased under oxidizing conditions (**Fig. 2A**). The amino acid sequence of AtSAL1 includes four cysteine residues as potential targets for redox regulation (Cys21, Cys119, Cys167, and Cys190). When these cysteine residues were mutated to redox-insensitive alanine residues, total activity decreased 50% but, more importantly, oxidative down-regulation of AtSAL1 activity was lost (**Fig. 2A**). The down-regulation of AtSAL1 activity coincided with the appearance of multiple protein bands on SDS-PAGE (**Fig. 2A**, bottom panels). Significantly, the multiple band patterns of oxidized AtSAL1 on SDS-PAGE was reversible upon addition of reducing agent (**Fig. 2B**); the altered migration of proteins with disulfide bond(s) due to intramolecular loop formation is well established (17, 18).

Combinatorial analysis of Cys to Ala mutations facilitated identification of the Cys pairs involved in the dominant disulfide bonded bands (**Fig. 2C**). This revealed two important features of the oxidation/inactivation process: first, full oxidation of recombinant AtSAL1 was not possible and only a fraction of the protein was converted to anomalously migrating oxidized bands; second, a specific, dominant, band that was observed when the WT protein was oxidized was lost when either Cys167 or Cys190 was mutated to Ala, suggesting that they form a disulfide bond. Kinetic analysis of Cys to Ala mutations showed that when Cys119 or Cys190

1 were mutated to Ala no loss of activity was observed in oxidizing conditions, suggesting that
2 Cys167-Cys190 and Cys119 may be required for inactivation of AtSAL1 (**Fig. 2A**).

3 To investigate this redox sensing mechanism in more detail, we subsequently crystallized and
4 solved the molecular structure of AtSAL1 to 3.05 Å resolution in its apo form (PDB 5ESY, **Fig.**
5 **3, Table S2**). AtSAL1 is an α/β protein belonging to the carbohydrate phosphatase fold and
6 superfamily (19) showing the closest structural homology to the yeast (*Saccharomyces*
7 *cerevisiae*) PAP phosphatase ortholog, ScHAL2 [PDB 1KA1(20), r.m.s.d for C α atoms = 2.4 Å,
8 with amino acid sequence identity of 37% as calculated by the DALI server (21)]. Interestingly,
9 we found that AtSAL1 crystallized as a dimer; a crystallographic 2-fold interface was clearly
10 visible and detected with the Protein Interfaces, Surfaces and Assemblies (PISA) server (22).
11 The dimer interface is centered on a symmetrical pair of Cys119 side chains from each monomer
12 in the dimer (**Fig. 3A**), suggesting a role for an intermolecular disulfide in dimerization. Each
13 monomer also contains a potential intramolecular Cys167-Cys190 disulfide pair located across
14 adjacent beta strands (**Fig. 3A**); such a cross-strand disulfide is often a metastable switch used to
15 control protein activity (23). Cys21 was not located near any potential disulfide bonding
16 partners. Notably, none of the cysteine residues are located in the vicinity of the active site,
17 suggesting that the regulation must be remote, or allosteric.

18 Although previously reported to be a monomer (24), we found that AtSAL1 exists in monomer-
19 dimer equilibrium in solution through size exclusion chromatography (SEC) and SEC-multi
20 angle laser light scattering (MALLS) (**Fig. 4A, Fig. S1**). Native PAGE analysis of recombinant
21 AtSAL1 reveals that the dimeric fraction is stable under oxidizing conditions, owing to the
22 presence of an intermolecular disulfide, but under sufficiently reducing conditions the protein
23 returns to equilibrium between monomer and dimer (**Fig. 4B**). Interestingly, the monomeric and

1 dimeric species displayed strikingly different redox sensitivity: whereas the monomer displayed
2 high catalytic activity and is resistant to oxidation and inactivation, the dimer is less active under
3 reducing conditions, but is extremely sensitive to oxidation and is rapidly inactivated, with
4 formation of disulfide bonds, including the intramolecular Cys167-Cys190 bond, in the presence
5 of oxidized DTT (**Fig. 4C, Table 1**). Thus, it appears that dimerization is a precursor to oxidative
6 inactivation, and that the oligomeric equilibrium can be altered under oxidizing conditions
7 through the formation of an intermolecular disulfide bridge. This result is consistent with the
8 data presented in **Fig. 2** showing that the mixed oligomeric species of AtSAL1 do not undergo
9 full oxidation owing to the resistance of monomer to oxidation, and that the Cys119 and Cys190
10 residues are involved in separate disulfide bonds that are both important for inactivation.

11 Given that dimerization appears to be essential for the intramolecular Cys167-Cys190 disulfide
12 bond formation, and that oxidation can inactivate AtSAL1, we sought to investigate the
13 mechanisms that underlie these processes. Allosteric regulation of protein activity is
14 commonplace (25), and frequently involves alteration of protein dynamics and trapping of
15 proteins in inactive conformations (26-29). Thus, we performed molecular dynamics (MD)
16 energy minimization to generate monomeric (reduced) and dimeric (oxidized) AtSAL1 models
17 to investigate the impact of dimerization and the disulfide bonds on the protein structure and
18 dynamics. Normal mode analysis of elastic network models (NMA-ENM) can effectively
19 predict and analyze large-scale collective motions in proteins (30, 31), and was used here to
20 investigate the impact of the Cys119-Cys119 and Cys167-Cys190 disulfide bridges and
21 dimerization on the flexibility of AtSAL1.

22 As shown in **Fig. 3B**, loop 1 overhangs the active site in an open conformation; the equivalent
23 loop to loop 1 in the AtSAL1 ortholog, ScHAL2, has been shown to close over the active site to

1 stabilize substrate (20). In AtSAL1, NMA-ENM indicates that loop 1 fluctuates between open
2 and closed conformations in a manner common to active site loops in almost all phosphatases
3 (**Fig. 3B**) (32, 33), suggesting that this movement is likely to be important for catalytic activity.
4 Loops 3 and 4 are located at the dimer interface and adjacent to loop 1, while loop 8 is also
5 adjacent to loop 1.

6 The mobility of these loops in the oxidized dimer and reduced monomer are strikingly different,
7 with loops 1, 3, 4, and 8 all being substantially rigidified through dimerization and disulfide bond
8 formation (**Fig. 3C**). The dynamic coupling of these loops is also significantly different between
9 the monomer and dimer, and these loops become significantly more hindered in the dimer (**Fig.**
10 **S2**). These data also allow a plausible explanation for the resistance of the monomer to
11 oxidation, since the formation of the Cys167- Cys190 disulfide bond will require the two
12 residues to be located in close proximity and to be relatively stable, which would be the case in
13 the dimer but not the monomer. Thus, the decreased activity of AtSAL1 in the
14 dimerized/oxidized state likely results from the rigidification of the active site loops,
15 allosterically inhibiting the enzyme by preventing it from adopting conformations that are
16 essential for activity and substrate binding. Indeed, both k_{cat} and K_{M} are affected by dimerization
17 and oxidation (**Table 1**). This result is consistent with the current view of allosteric inhibitory
18 regulation of proteins (28, 29), and provides a rapid means of reversible enzyme inactivation.

19 **Formation of the intramolecular disulfide bond controlling AtSAL1 activity can be** 20 **mediated by the chloroplast redox buffer GSH/GSSG**

21 We then investigated whether *in vitro* AtSAL1 inactivation by the redox regulatory mechanisms
22 shown in **Fig. 3** can be induced by *in vivo* redox couples present in the chloroplast, such as

glutathione (GSH). During oxidative stress GSH can be oxidized to oxidized glutathione (GSSG). GSSG is known to glutathionylate cysteine residues of chloroplast proteins to regulate their activity (3), and it promotes formation of an intramolecular disulfide bond between proximal cysteine residues *via* thiol-disulfide exchange (34) (**Fig. S3**). Therefore, we tested whether glutathionylation may also induce formation of the Cys167-Cys190 bond in AtSAL1. The GSSG-treated AtSAL1 was able to form the Cys167-Cys190 disulfide in all recombinant proteins containing both residues (**Fig. 5A**). Additionally, decreased activity in GSSG-treated AtSAL1 correlated with glutathionylation of Cys119 and Cys190 as detected by mass-spectrometry (**Fig. 5B**). Critically, glutathionylation down-regulated activity in both monomeric and dimeric AtSAL1 samples (**Fig. 5C**). The redox titration of both monomeric and dimeric AtSAL1 with GSH/GSSG yielded redox midpoint potentials (E_m) close to the physiological glutathione redox potential (-317 ± 8 mV) in *Arabidopsis* chloroplasts (35) (**Fig. 5C**). Therefore, two redox processes can decrease AtSAL1 activity: the first involving dimerization and intermolecular disulfide bonding, and the second a dimerization-independent process involving glutathionylation by the chloroplast redox couple GSH/GSSG. Both mechanisms result in the formation of the Cys167-Cys190 intramolecular disulfide and down-regulation of AtSAL1 activity.

In vitro* redox regulatory mechanisms of AtSAL1 are recapitulated *in vivo

If the SAL1-PAP pathway is a primary regulator of PRANGs, and PAP concentrations are controlled by redox regulation of SAL1 as hypothesized, then the multiple redox mechanisms regulating AtSAL1 *in vitro* should be recapitulated *in vivo* in response to chloroplast redox cues that initiate PRANG regulation. We tested this hypothesis by analyzing AtSAL1 activity, and

intramolecular disulfide formation and dimerization, when photosynthetic ROS and the chloroplast redox state were manipulated in various ways.

First, we observed *in vivo* formation of the characteristic Cys167-Cys190 disulfide band in AtSAL1 during drought stress. *In vivo* abundance of the Cys167-C190 disulfide bonded form of AtSAL1 progressively increased in correlation with decreasing AtSAL1 activity and increasing PAP accumulation in leaves of drought-stressed *Arabidopsis* (**Fig. 6A**). Second, across the multiple abiotic stress treatments that increase abundance of PSI-sourced ROS and lead to reduction of *in vivo* AtSAL1 activity shown in **Fig. 1A**, the proportion of dimeric AtSAL1 in oxidatively-stressed *Arabidopsis* leaves increased relative to control (**Fig. 6B**). This is in agreement with the observed Cys119 intermolecular disulfide-mediated dimerization under oxidative conditions (**Fig. 4B**).

To complement the *in vivo* results shown in **Fig. 6**, either one of two approaches can demonstrate that redox regulation of AtSAL1 enables PAP accumulation and PRANG expression. First, AtSAL1 Cys-Ala mutants that are redox-insensitive *in vitro* can be expressed in *Arabidopsis*, however abundance of the Cys-Ala proteins were lower than WT when expressed in *E. coli* (**Fig. S4**). It is well established in plants that point mutations, let alone four mutations in a single gene, can affect a variety of protein characteristics, including *in vivo* stability, activity, and/or protein-protein interactions (36). Indeed, two other SAL1 point mutations, *alx8* and *hos2*, affect protein stability and activity in a temperature-dependent manner, respectively (37, 38).

A second approach involves analyzing the same gene across many species to identify strong conservation of the same characteristic, which would indicate strong evolutionary selection to maintain this function (39, 40). The SAL1-PAP pathway for PRANG regulation and stress

1 tolerance is functional across dicotyledonous (9, 37) and monocotyledonous plants (16).
2 Therefore, if AtSAL1 is genuinely redox-regulated *in vivo*, then the cysteine residues conferring
3 *in vitro* redox sensitivity in AtSAL1 should be strongly conserved in evolution beyond
4 *Arabidopsis* to other plant species; and distantly-related orthologs should also show redox-
5 sensitive biochemical activity.

6 We found that the redox-responsive cysteine residues in AtSAL1 are indeed highly conserved
7 (**Fig. S5**). The Cys167-C190 intramolecular disulfide pair is strongly conserved across the
8 representative bryophyte, chlorophyte, early angiosperm, eudicot and monocot species
9 examined. The Cys119 residue that mediates the intermolecular dimerization is less conserved,
10 but is still present in 33% of eudicot SAL1 orthologs and in two monocot proteins. In the
11 distantly related *Poaceae* SAL1 orthologs including the *Oryza sativa* SAL1 (OsSAL1) protein,
12 the position of the conserved AtSAL1 Cys190 is C-terminally shifted by 7 amino acids.
13 Interestingly, these proteins possess an additional conserved cysteine residue (**Fig. S5**).

14 We investigated OsSAL1 in detail, given that it has been shown to have activity against PAP
15 (41), and monocots are estimated to have diverged from dicots 140 – 150 million years ago (42).
16 Conserved similarities in redox sensitivity between dicot AtSAL1 and monocot OsSAL1 would
17 therefore be functionally and evolutionarily significant. As was observed for AtSAL1, OsSAL1
18 activity is inhibited by oxidation (**Table 2**) and redox titration of the protein shows a
19 physiologically-relevant E_m (**Fig. 7A**). OsSAL1 conformation can also be modified by
20 glutathionylation (**Fig. 7B**). Homology modelling of OsSAL1 reveals that both the strongly
21 conserved cysteine residues are surface-exposed (**Fig. 7C**), which may potentiate redox
22 regulation.

1 Finally, a corollary to the results described above is that if a SAL1 ortholog lacks the redox-
2 responsive cysteine residues, then introduction of these residues should enhance redox sensitivity
3 in the new protein. The activity of the yeast (*Saccharomyces cerevisiae*) ortholog, ScHAL2,
4 shows some redox-sensitivity to glutathionylation (**Table S3**), possibly due to presence of a
5 surface-exposed cysteine (**Fig. S6A**). However, ScHAL2 lacks the three cysteines at positions
6 structurally equivalent to those of AtSAL1, including the Cys119 side chain that promotes
7 dimerization (**Fig. S5**) and the Cys167-Cys190 intramolecular disulfide (**Fig. 8A**). This suggests
8 that the redox-sensing mechanisms regulating AtSAL1 activity in plants (**Figs. 1-6**) are absent in
9 yeast, and may have evolved in plants for chloroplast redox sensing and PRANG regulation. We
10 therefore introduced three additional cysteine residues (Thr21Cys, Phe127Cys, Tyr196Cys) into
11 ScHAL2 (ScHAL2+3C).

12 Phe127Cys is the equivalent of AtSAL1 Cys119 that promotes dimerization, while Tyr196Cys
13 introduces a potential disulfide pair in the same position as the critical intramolecular disulfide
14 that regulates activity of the dimeric AtSAL1 (**Fig. 8A**). Indeed, ScHAL2+3C showed
15 significantly greater redox sensitivity compared to WT ScHAL2 *in vitro* (**Fig. 8B, Table S3**).
16 When expressed *in vivo*, the engineered ScHAL2+3C was as efficient as WT ScHAL2 in
17 degrading PAP under unstressed conditions (**Fig. S6B**). Critically, introduction of the
18 intramolecular disulfide also increases redox sensitivity *in vivo* compared to the WT form: yeast
19 *Δhal2* overexpressing ScHAL2+3C significantly accumulated PAP when challenged with mild
20 H₂O₂ stress, whereas those overexpressing WT ScHAL2 did not (**Fig. 8C**). Thus, addition of the
21 cysteine residues alone is sufficient to induce enhanced redox sensitivity to the yeast SAL1
22 ortholog.

Discussion

Redox regulation of AtSAL1 involves multiple structural mechanisms

A diverse range of proteins are specifically regulated by disulfide formation (23). The Cys167-Cys190 intramolecular disulfide in AtSAL1 is intriguing because it occurs across two antiparallel beta-strands immediately adjacent to one another, at the base of a hairpin loop connecting these strands (**Fig. 3A**). Formation of a disulfide across adjacent beta strands is a form of Cross-Strand Disulfide (CSD) that have been termed ‘forbidden disulfides’(23), since they disobey the established rules of protein stereochemistry (43, 44) and introduce strain into the protein structure that may be energetically and structurally unfavorable (44). However, recent findings indicate that strain in local areas of a protein are tolerated for regulation of protein function (23). An increasing number of proteins have been characterized that contain CSDs; in most cases, these disulfides regulate function (23). These examples include proteins involved in chloroplast redox control such as thioredoxins (TRXs), which have a canonical CSD-containing motif that is strongly conserved across evolution (23, 45). CSD formation directly blocks catalytic cysteines in thioredoxins (46, 47), whereas the CSD decreases protein flexibility in AtSAL1 (**Fig. 3**). Formation of the intramolecular Cys167-Cys190 disulfide in response to oxidizing conditions is dependent upon dimerization (**Fig. 4C**), which stabilizes the protein conformation (**Fig. 3**). The dimerization interface between AtSAL1 monomeric subunits is relatively small (**Fig. 3A**), which may result in a relatively weak or transient interaction *in vivo* and explain the monomer-dimer equilibrium in solution under reducing conditions, until the interface is locked together through the Cys119-Cys119 intermolecular disulfide bonding during oxidative stress. Interestingly, the inactivation of both monomeric and dimeric AtSAL1 by GSH/GSSG, and formation of the

Cys167-Cys190 disulfide by glutathionylation *via* thiol-disulfide exchange (**Fig. 5**), reveals an additional mechanism for redox regulation of AtSAL1.

AtSAL1 redox regulation allows both metabolic control of sulfur assimilation and oxidative stress signaling

The flux of sulfur in plants is regulated partly *via* redox control of key enzymes in the sulfur assimilation pathway (48-50). Oxidative stress is expected to increase sulfur flux into sulfur reduction for production of the redox buffer GSH/GSSG, as two key enzymes in this primary branch of sulfur metabolism, APS reductase (APR) and Glutamate-Cysteine Ligase (GCL) are more active when oxidized (49, 50). Conversely, PAP biosynthesis in the parallel, secondary pathway should be down-regulated by oxidative stress since enzymatic synthesis of the PAP precursor, PAPS, by APS kinase (APK) is decreased by oxidation (48).

Within the present study we show that AtSAL1 is significantly less active when oxidized (**Figs. 1-6**), thus providing a mechanism for the 30-fold accumulation of PAP seen in WT plants during drought (9), without necessitating increased sulfur allocation into secondary sulfur metabolism and PAP synthesis. We also show that metabolites from one sulfur metabolism branch can influence biosynthesis of metabolites in the parallel pathway, since GSH/GSSG directly regulates AtSAL1 activity (**Fig. 5**) and hence PAP levels. Significantly, the redox midpoint potential (E_m) of AtSAL1 (-308 ± 2 mV for monomer and -284 ± 5 mV for dimer at pH 7.5; **Fig. 5C**) overlaps with those determined for the oxidation-activated primary sulfur metabolism (GSH/GSSG) enzymes ($-330\text{mV} \pm 10\text{mV}$ at pH 8.0 for APR and -318 ± 11 mV at pH 7.0 for GCL) (49, 50) and oxidation-inhibited secondary sulfur metabolism (PAPS/PAP) APK enzymes (-286 ± 18 mV at pH 7.5) (48). Therefore, the same redox state in chloroplasts can concomitantly

1 regulate multiple sulfur metabolism enzymes including AtSAL1. This could allow coordination
2 of flux through the sulfur pathway for redox buffering (GSH/GSSG) concomitant to stress
3 signaling (PAP).

4 The redox-responsive cysteine residues in AtSAL1 are conserved in plant species that lack
5 glucosinolate biosynthesis, which constitute a major sink for sulfur (and source of PAP) in
6 *Arabidopsis* and its relatives in the *Brassicaceae* (14) (**Fig. S5**). Indeed, the redox regulation was
7 conserved in OsSAL1 (**Fig. 7**), despite *O. sativa* being monocotyledonous and lacking
8 glucosinolates. Another indication that the SAL1-PAP pathway functions independently of
9 glucosinolates is that it also mediates stress tolerance in wheat (16). Therefore, the redox
10 regulation of SAL1 can be uncoupled from sulfur metabolism.

11 **SAL1 acts as a general redox sensor in the chloroplast for retrograde signaling and** 12 **PRANG regulation**

13 Our results indicate that SAL1 activity in plants is sensitive to the overall redox state of the
14 chloroplast and not to a specific stimulus or sensor protein (**Fig. 1**). The SAL1 protein is
15 sensitive to ROS production and redox state of PSI, where O_2^- is produced and detoxified via
16 Superoxide Dismutase (SOD)-mediated dismutation to H_2O_2 , which is further detoxified by
17 thylakoidal and stromal APXs (tAPX and sAPX). Deficiency in sAPX compromises H_2O_2
18 degradation and concomitantly increases O_2^- abundance at PSI due to SOD inhibition (1); this
19 increased the effect of HL stress on suppression of AtSAL1 activity (**Fig. 1B**). Indeed, direct
20 induction of O_2^- production at PSI by methyl viologen inhibited AtSAL1 (**Fig. 1A**). Perturbing
21 multiple aspects of chloroplast redox homeostasis also influenced AtSAL1 activity (**Fig. 1B**).
22 This includes the major oxidized protein regeneration pathway in chloroplasts involving

1 NADPH-dependent Thioredoxin Reductase C (NTRC) (51), and the redox buffers NADPH
2 /NADP⁺ and GSH / GSSG. Mutants in these pathways are unsurprisingly hypersensitive to
3 oxidative stress (52, 53), but also deregulated in PRANG expression during stress (54). The latter
4 probably reflects the influence of redox poise on AtSAL1 activity and PAP accumulation.

5 The convergence of photosynthetic ROS and redox cues on SAL1 has key implications for stress
6 retrograde signaling and regulation of PRANGs. Our results here demonstrating the coupling of
7 SAL1 activity and PAP accumulation to chloroplastic redox poise presents this enzyme as an
8 unconventional oxidative stress sensor and hub for the convergence of H₂O₂, O₂⁻ and redox cues
9 in the chloroplast that alter nuclear gene expression (4, 6, 7). That is, the primary function of
10 SAL1 is not to sense ROS and redox state, yet its sensitivity to these chloroplast cues enables
11 them to be sensed by the nucleus *via* PAP, providing capacity for fine-tuning responses. Such a
12 hypothesis does not preclude parallel pathways that also sense or respond to ROS or redox state
13 in the chloroplast. For example, recent evidence shows that projections from chloroplasts called
14 stromules increase in abundance during stress and can enable transport of ROS from chloroplasts
15 to the nucleus (55, 56). The extent to which PAP and other ROS communication pathways
16 overlap is a subject of future research.

17 The conserved secondary redox sensing by SAL1 suggests that these enzymes may be
18 considered ‘moonlighting’ proteins (57). Many moonlighting proteins are evolutionarily-
19 ubiquitous enzymes that have secondary functions in diverse processes including metabolism
20 and disease (57). Intriguingly, to our knowledge SAL1 would constitute the first moonlighting
21 oxidative stress sensor described in plants. The sensitivity of the sensor may be fine-tuned
22 differently across evolution to fulfill kingdom-specific functions, since Arabidopsis and rice

1 SAL1 appears more responsive to ROS and redox state than yeast HAL2 due to presence of the
2 intramolecular Cys167-Cys190 disulfide (**Figs. 3A, 8B-C, Table S3**).

3 Whether chloroplast communication necessitates additional layers of complexity in regulation of
4 SAL1 in plants requires further elucidation. Regardless, there is precedent for the evolution of
5 increased redox sensitivity in PAP/PAPS metabolism in plants. For instance, the adenosine 5'-
6 phosphosulfate kinase (APK) enzyme catalyzing PAPS production evolved increased redox
7 sensitivity in the transition from cyanobacteria to higher plants (58). It is also fascinating that
8 WT ScHAL2 shares some conservation of redox-sensitivity (**Fig. 8, Table S3**), albeit to a lesser
9 extent, with AtSAL1 despite lacking the AtSAL1 redox-responsive cysteine residues. Instead,
10 ScHAL2 may be regulated *via* a different surface-exposed cysteine residue (**Fig. S6**). It may be
11 that PAP phosphatases in other kingdoms are redox-regulated *via* analogous mechanisms
12 targeting different cysteine residues, and this will be interesting to explore.

13 In summary, transient elevation of PAP levels as an oxidative stress signal in plants is coupled to
14 the redox state perceived by SAL1. That at least four different ROS/redox couples (H_2O_2 , O_2^- ,
15 GSH/GSSG and $\text{DTT}_{\text{red}}/\text{DTT}_{\text{ox}}$) regulate SAL1 enables a fine-tuning of SAL1 activity and thus
16 retrograde signaling to communicate the different fluctuations of chloroplast ROS balance/redox
17 poise in response to environmental stimuli. It is intriguing that a similarity in regulation of SAL1
18 orthologs relates more to the secondary function of redox sensing and stress signaling than
19 sulfation, and raises the question as to which function was the primary driver for evolutionary
20 conservation of this protein. Our results suggest that dual-function SAL1 orthologs may be
21 uniquely positioned as single-component integrators of sensing and signaling of aspects of
22 oxidative stress in plants.

Materials and Methods

Plant material and growth conditions

Arabidopsis seeds were germinated on soil and kept at 4 °C for 3 days to synchronize germination. Plants were grown at 100-150 $\mu\text{mol photons m}^{-2} \text{ s}^{-1}$, 12 h photoperiod, 21-23 °C and 50-55 % humidity. Five-week old plants were used for all stress assays (**SI Text**). T-DNA insertion lines for the redox homeostasis mutants *sapx* (1), *ntrc* (52), *phs1* (53), and *cos1* (59) (**Table S1**) were obtained from the Arabidopsis Biological Resource Centre (ABRC). The amiRNA silencing line for tAPX (1) was provided by Prof. Christophe Laloi (Aix-Marseille) and *rax1-1* (54) was obtained from Prof. Phil Mullineaux (Essex) (**Table S1**).

Protein purification from biological samples

Arabidopsis leaf native proteins were extracted using a protocol modified from Murguia *et al.* (60) (**SI Text**). Native proteins were kept on ice and used immediately in Clear-Native PAGE and activity assays, as described later.

For detection of the Cys167-Cys190 intramolecular disulfide in endogenous AtSAL1, native proteins were incubated with 10 mM iodoacetamide in the dark for 1 h to prevent oxidation of any cysteines that were reduced *in vivo*. Leaf protein was then precipitated in TCA / acetone, washed twice with cold acetone and resuspended in solubilisation buffer (9 M urea, 4 % (w/v) CHAPS, 1 % (w/v) DTT, 35 mM Tris base) before SDS-PAGE and western blotting (**SI Text**).

Recombinant protein purification

Recombinant WT AtSAL1 protein was expressed in *Escherichia coli* BL21 DE3 cells (New England BioLabs, USA) and purified using standard metal affinity purification (**SI Text**). The

purified recombinant proteins were stored in storage buffer [50 mM Tris-HCl pH 8.0, 150 mM NaCl, 20 mM KCl, 1 mM MgCl₂, 15% glycerol] at -80 °C.

Protein gel electrophoresis

Recombinant protein, 0.5-1 µg, was incubated in degassed storage buffer [50 mM Tris-HCl pH 8.0, 150 mM NaCl, 50 mM KCl, 1 mM MgCl₂, 15% glycerol] in the presence of either 5 mM DTT_{red} (reducing conditions) or 5mM DTT_{ox} (trans-4,5-Dihydroxy-1,2-dithiane; oxidizing conditions) for 1 hour at RT, then resolved by SDS-PAGE and stained as described in **SI Text**.

To visualize effects of GSH/GSSG, proteins were incubated in degassed storage buffer containing 20mM GSH or 20mM GSSG, then run on gels and stained as before.

For Clear-Native PAGE, proteins were incubated with redox agents as above but resuspended in Native Sample Loading buffer [100 mM Tris-HCl, 10 % glycerol, 0.0025 % bromophenol blue, pH 8.6) and resolved on a 3-12 % Novex NativePAGE gel (Life Technologies, USA) in Native Running Buffer [25 mM Tris, 192 mM Glycine, pH 8.3] without denaturing agents.

Activity assays

Recombinant protein activity against PAP was assayed by incubating 0.2 µg protein in degassed Activity Buffer [100 mM Tris-MES pH 7.5, 1 mM Mg acetate] in presence of either reducing or oxidizing equivalents of DTT_{red}/DTT_{ox} (5 mM) or GSH/GSSG (20mM) for 1 hour at 25 °C, then increasing concentrations of PAP was added to a final volume of 150 µL and initial activity assayed at 25 °C (AtSAL1 and OsSAL1) or 30 °C (SchAL2). The reaction was stopped by flash-freezing in liquid N₂. AMP produced from degradation of PAP was quantified using the method for derivatization and detection of adenosines *via* High Performance Liquid Chromatography as previously described (9). All Michaelis-Menten kinetics parameters were calculated using

GraphPad Prism (GraphPad Software Inc., USA). For redox titration of activity, SAL1 protein was incubated as above with different ratios of DTT_{red}:DTT_{ox} (final total concentration of 5 mM) or GSH:GSSG (final concentration of 20 mM). Values for redox midpoint potential, E_m, was calculated by fitting titration data to the Nernst equation using GraphPad Prism:

$$E_h = E_m + (RT/nF)(\ln ([GSSG]/[GSH]^2)) \text{ for glutathione}$$

And

$$E_h = E_m + (RT/nF)(\ln ([DTT_{ox}]/[DTT_{red}])) \text{ for DTT}$$

with an RT/F of 25.7mV and n=2 (49, 61)

For activity of AtSAL1 in native protein extracts from *Arabidopsis*, 10 µg of total native protein extract was incubated in the same Activity Buffer as above with increasing concentrations of PAP at 25 °C without any redox agents.

Crystallization, data collection and refinement

AtSAL1 crystals were grown by vapor-diffusion in hanging-drops. Crystals formed at a protein concentration of 20 mg/ml in 20-30 % PEG 2000-MME, 0.2 M (NH₄)₂SO₄, 0.1 M HEPES pH 8.0 – 8.6. Diffraction data were collected at the Australian Synchrotron at the MX2 beamline (λ = 0.9537 Å). The resolutions limits of the data were assessed on the basis of the significance of the CC_{1/2} at the *P*=0.001 level (62, 63). Diffraction data were integrated using XDS (64) and scaled using *SCALA* from the CCP4 program suite (65). The crystals belonged to the *P*6₁ space group and significant merohedral twinning was identified by xtriage (66)(twin operator h,-h-k,-l). Phases were obtained by molecular replacement in Phaser (67) using the yeast ortholog of SAL1 (PDB 1QGX) (20) as the search model. The crystallographic asymmetric unit contained two copies of SAL1. Twin refinement was completed in Phenix (66, 68).

Simulation of the oxidized AtSAL1 dimer

The intermolecular (Cys119-Cys119) and intramolecular (Cys167-Cys190) disulfides were modelled using the GROMACS package (69) in conjunction with the GROMOS 53a7 force-field for condensed phases (70). To prepare the model, the crystallographic coordinates of the AtSAL1 dimer were immersed in a cubic shaped box of solvent with a minimum of 1 nm between the protein and the box edge. The simple point charge model was used to represent water (71) and the protein's charge was neutralized by the addition of sodium ions. Electrostatic energy was calculated using the particle mesh Ewald (PME) method (72) and cut-off distances for the calculation of van der Waals and Coulomb interactions were set at 0.9 and 1.4 nm, respectively. To model the disulfide bonds between Cys167-Cys190 and Cys119-Cys119 the AtSAL1 topology file was edited to include a bond between the sulfur atoms of the cysteines. The resulting system was energy minimized via steepest descent to the limit of machine precision. During energy minimization the disulfide bond length decreased to an appropriate length (2 ± 0.2 Å). For comparison the reduced AtSAL1 monomer was modelled. To prepare the model the crystallographic coordinates of each monomer in the AtSAL1 asymmetric unit were energy minimized. The same procedure was used to energy minimize the monomeric structure as the dimeric structure, except disulfide bonds (Cys167-Cys190) were not included in the monomer. To obtain an estimate of the flexibility of the energy minimized structures the structures were submitted to the iMOD normal mode analysis webserver (73). To analyze the coupling of AtSAL1 motions the covariance of C_{α} motions were plotted (74).

Acknowledgments: We thank Prof. Ian Dawes (University of New South Wales) for providing the yeast strains, as well as Dr Derek Collinge, Mr Diep Ganguly and Miss Nay Chi Khin

(ANU) for technical support. We thank Dr Paul D. Carr for assistance with crystallization and helpful discussions. We received financial support from the ARC Centre of Excellence in Plant Energy Biology (CE140100008) and scholarships to KXC (IPRS, ANU) and SYP (ANU). This research was also supported by the Wellcome Trust (project grant 092283, to W.A.) and the European Commission (Marie Cure Fellowship 625451, to J.W.M.).

Author contributions: Performed experiments: K.X.C., P.D.M., S.Y.P., J.W.M., N.N., E.S., J.G., T.G. Study design and data analysis: K.X.C., P.D.M., W.A., G.M.E., C.J.J., B.J.P. Manuscript preparation: K.X.C., P.D.M., C.J.J., B.J.P. All authors discussed the results and commented on the manuscript.

Author information: Crystal structure data is deposited at PDB (PDB ID: 5ESY). The authors declare no competing financial interests. Correspondence and requests for materials should be addressed to B.J.P. (barry.pogson@anu.edu.au).

References

1. Asada K (1999) The Water-Water Cycle In Chloroplasts: Scavenging of Active Oxygens and Dissipation of Excess Photons. *Annu Rev Plant Physiol Plant Mol Biol* 50:601-639.
2. Pesaresi P, *et al.* (2009) Arabidopsis STN7 kinase provides a link between short- and long-term photosynthetic acclimation. *Plant Cell* 21(8):2402-2423.
3. Michelet L, *et al.* (2005) Glutathionylation of chloroplast thioredoxin f is a redox signaling mechanism in plants. *Proc Natl Acad Sci U S A* 102(45):16478-16483.
4. Gadjev I, *et al.* (2006) Transcriptomic Footprints Disclose Specificity of Reactive Oxygen Species Signaling in Arabidopsis. *Plant Physiology* 141(2):436-445.
5. Laloi C, *et al.* (2007) Cross-talk between singlet oxygen- and hydrogen peroxide-dependent signaling of stress responses in Arabidopsis thaliana. *Proc Natl Acad Sci U S A* 104(2):672-677.
6. Chi W, Sun XW, & Zhang LX (2013) Intracellular Signaling from Plastid to Nucleus. *Annual Review of Plant Biology*, Vol 64 64:559-582.
7. Chan KX, Phua SY, Crisp P, McQuinn R, & Pogson BJ (2015) Learning the Languages of the Chloroplast: Retrograde Signaling and Beyond. *Annu Rev Plant Biol*.
8. Ramel F, *et al.* (2012) Carotenoid oxidation products are stress signals that mediate gene responses to singlet oxygen in plants. *Proc Natl Acad Sci U S A* 109(14):5535-5540.
9. Estavillo GM, *et al.* (2011) Evidence for a SAL1-PAP chloroplast retrograde pathway that functions in drought and high light signaling in Arabidopsis. *Plant Cell* 23(11):3992-4012.

- 1 10. Karpinski S, Escobar C, Karpinska B, Creissen G, & Mullineaux PM (1997) Photosynthetic electron
2 transport regulates the expression of cytosolic ascorbate peroxidase genes in Arabidopsis during excess
3 light stress. *Plant Cell* 9(4):627-640.
- 4 11. Karpinski S, *et al.* (1999) Systemic Signaling and Acclimation in Response to Excess Excitation Energy in
5 Arabidopsis. *Science* 284(5414):654-657.
- 6 12. Rossel JB, *et al.* (2007) Systemic and intracellular responses to photooxidative stress in Arabidopsis. *Plant*
7 *Cell* 19(12):4091-4110.
- 8 13. Tikkanen M, Gollan PJ, Suorsa M, Kangasjarvi S, & Aro EM (2012) STN7 Operates in Retrograde
9 Signaling through Controlling Redox Balance in the Electron Transfer Chain. *Front Plant Sci* 3:277.
- 10 14. Chan KX, Wirtz M, Phua SY, Estavillo GM, & Pogson BJ (2013) Balancing metabolites in drought: the
11 sulfur assimilation conundrum. *Trends Plant Sci* 18(1):18-29.
- 12 15. Lee BR, *et al.* (2012) Effects of *fou8/fry1* mutation on sulfur metabolism: is decreased internal sulfate the
13 trigger of sulfate starvation response? *PLoS ONE* 7(6):e39425.
- 14 16. Manmathan H, Shaner D, Snelling J, Tisserat N, & Lapitan N (2013) Virus-induced gene silencing of
15 Arabidopsis thaliana gene homologues in wheat identifies genes conferring improved drought tolerance. *J*
16 *Exp Bot* 64(5):1381-1392.
- 17 17. Després C, *et al.* (2003) The Arabidopsis NPR1 Disease Resistance Protein Is a Novel Cofactor That
18 Confers Redox Regulation of DNA Binding Activity to the Basic Domain/Leucine Zipper Transcription
19 Factor TGA1. *Plant Cell* 15(9):2181-2191.
- 20 18. Wood MJ, Andrade EC, & Storz G (2003) The Redox Domain of the Yap1p Transcription Factor Contains
21 Two Disulfide Bonds. *Biochemistry* 42(41):11982-11991.
- 22 19. Murzin AG, Brenner SE, Hubbard T, & Chothia C (1995) SCOP: a structural classification of proteins
23 database for the investigation of sequences and structures. *J Mol Biol* 247(4):536-540.
- 24 20. Albert A, *et al.* (2000) X-ray structure of yeast hal2p, a major target of lithium and sodium toxicity, and
25 identification of framework interactions determining cation sensitivity. *Journal of Molecular Biology*
26 295(4):927-938.
- 27 21. Holm L & Rosenström P (2010) Dali server: conservation mapping in 3D. *Nucleic Acids Research* 38(Web
28 Server issue):W545-W549.
- 29 22. Krissinel E & Henrick K (2007) Inference of Macromolecular Assemblies from Crystalline State. *Journal*
30 *of Molecular Biology* 372(3):774-797.
- 31 23. Wouters MA, Fan SW, & Haworth NL (2010) Disulfides as redox switches: from molecular mechanisms to
32 functional significance. *Antioxid Redox Signal* 12(1):53-91.
- 33 24. Peltier JB, *et al.* (2006) The oligomeric stromal proteome of *Arabidopsis thaliana* chloroplasts. *Mol Cell*
34 *Proteomics* 5(1):114-133.
- 35 25. Changeux J-P & Edelstein SJ (2005) Allosteric Mechanisms of Signal Transduction. *Science*
36 308(5727):1424-1428.
- 37 26. Li M, Smith CJ, Walker MT, & Smith TJ (2009) Novel Inhibitors Complexed with Glutamate
38 Dehydrogenase: Allosteric Regulation by Control of Protein Dynamics. *Journal of Biological Chemistry*
39 284(34):22988-23000.
- 40 27. Palmer AG (2015) Enzyme Dynamics from NMR Spectroscopy. *Accounts of Chemical Research*
41 48(2):457-465.
- 42 28. Guarnera E & Berezovsky IN (2015) Allosteric sites: remote control in regulation of protein activity. *Curr*
43 *Opin Struct Biol* 37:1-8.
- 44 29. Motlagh HN, Wrabl JO, Li J, & Hilser VJ (2014) The ensemble nature of allostery. *Nature* 508(7496):331-
45 339.
- 46 30. Bahar I & Rader AJ (2005) Coarse-grained normal mode analysis in structural biology. *Curr Opin Struct*
47 *Biol* 15(5):586-592.
- 48 31. López-Blanco JR, Aliaga JI, Quintana-Ortí ES, & Chacón P (2014) iMODS: internal coordinates normal
49 mode analysis server. *Nucleic Acids Research*.
- 50 32. Wiesmann C, *et al.* (2004) Allosteric inhibition of protein tyrosine phosphatase 1B. *Nat Struct Mol Biol*
51 11(8):730-737.
- 52 33. Choe JY, Fromm HJ, & Honzatko RB (2000) Crystal structures of fructose 1,6-bisphosphatase: mechanism
53 of catalysis and allosteric inhibition revealed in product complexes. *Biochemistry* 39(29):8565-8574.
- 54 34. Foyer CH & Noctor G (2011) Ascorbate and Glutathione: The Heart of the Redox Hub. *Plant Physiology*
55 155(1):2-18.

35. Maughan SC, *et al.* (2010) Plant homologs of the Plasmodium falciparum chloroquine-resistance transporter, PfCRT, are required for glutathione homeostasis and stress responses. *Proc Natl Acad Sci U S A* 107(5):2331-2336.
36. Bartlett M & Whipple C (2013) Protein change in plant evolution: tracing one thread connecting molecular and phenotypic diversity. *Frontiers in Plant Science* 4.
37. Wilson PB, *et al.* (2009) The nucleotidase/phosphatase SAL1 is a negative regulator of drought tolerance in Arabidopsis. *The Plant Journal* 58(2):299-317.
38. Xiong L, Lee H, Huang R, & Zhu JK (2004) A single amino acid substitution in the Arabidopsis FIERY1/HOS2 protein confers cold signaling specificity and lithium tolerance. *Plant J* 40(4):536-545.
39. Studer Romain A, Dessailly Benoit H, & Orengo Christine A (2013) Residue mutations and their impact on protein structure and function: detecting beneficial and pathogenic changes. *Biochemical Journal* 449(3):581-594.
40. Mularoni L, Ledda A, Toll-Riera M, & Albà MM (2010) Natural selection drives the accumulation of amino acid tandem repeats in human proteins. *Genome Research* 20(6):745-754.
41. Peng Z & Verma DPS (1995) A Rice HAL2-like Gene Encodes a Ca²⁺-sensitive 3'(2'),5'-Diphosphonucleoside 3'(2')-Phosphohydrolase and Complements Yeast met22 and Escherichia coli cysQ Mutations. *Journal of Biological Chemistry* 270(49):29105-29110.
42. Chaw SM, Chang CC, Chen HL, & Li WH (2004) Dating the monocot-dicot divergence and the origin of core eudicots using whole chloroplast genomes. *J Mol Evol* 58(4):424-441.
43. Richardson JS (1981) The anatomy and taxonomy of protein structure. *Adv Protein Chem* 34:167-339.
44. Thornton JM (1981) Disulphide bridges in globular proteins. *Journal of Molecular Biology* 151(2):261-287.
45. Collet J-F & Messens J (2010) Structure, Function, and Mechanism of Thioredoxin Proteins. *Antioxidants & Redox Signaling* 13(8):1205-1216.
46. Jeng MF, *et al.* (1994) High-resolution solution structures of oxidized and reduced Escherichia coli thioredoxin. *Structure* 2(9):853-868.
47. Qin J, Clore GM, & Gronenborn AM (1994) The high-resolution three-dimensional solution structures of the oxidized and reduced states of human thioredoxin. *Structure* 2(6):503-522.
48. Ravilious GE, Nguyen A, Francois JA, & Jez JM (2012) Structural basis and evolution of redox regulation in plant adenosine-5'-phosphosulfate kinase. *Proc Natl Acad Sci U S A* 109(1):309-314.
49. Hicks LM, *et al.* (2007) Thiol-Based Regulation of Redox-Active Glutamate-Cysteine Ligase from Arabidopsis thaliana. *Plant Cell* 19(8):2653-2661.
50. Bick J-A, *et al.* (2001) Regulation of the Plant-type 5'-Adenylyl Sulfate Reductase by Oxidative Stress. *Biochemistry* 40(30):9040-9048.
51. Nikkanen L & Rintamäki E (2014) Thioredoxin-dependent regulatory networks in chloroplasts under fluctuating light conditions. *Philosophical Transactions B* 369(1640).
52. Serrato AJ, Pérez-Ruiz JM, Spinola MC, & Cejudo FJ (2004) A Novel NADPH Thioredoxin Reductase, Localized in the Chloroplast, Which Deficiency Causes Hypersensitivity to Abiotic Stress in Arabidopsis thaliana. *Journal of Biological Chemistry* 279(42):43821-43827.
53. Ouyang M, *et al.* (2010) The photosensitive pbs1 mutant is impaired in the riboflavin biogenesis pathway. *Journal of Plant Physiology* 167(17):1466-1476.
54. Ball L, *et al.* (2004) Evidence for a direct link between glutathione biosynthesis and stress defense gene expression in Arabidopsis. *Plant Cell* 16(9):2448-2462.
55. Brunkard JO, Runkel AM, & Zambryski PC (2015) Chloroplasts extend stromules independently and in response to internal redox signals. *Proc Natl Acad Sci U S A* 112(32):10044-10049.
56. Caplan Jeffrey L, *et al.* (2015) Chloroplast Stromules Function during Innate Immunity. *Developmental Cell* 34(1):45-57.
57. Huberts DH & van der Klei IJ (2010) Moonlighting proteins: an intriguing mode of multitasking. *Biochim Biophys Acta* 1803(4):520-525.
58. Herrmann J, Nathin D, Lee SG, Sun T, & Jez JM (2015) Recapitulating the Structural Evolution of Redox Regulation in Adenosine 5' -Phosphosulfate Kinase from Cyanobacteria to Plants. *Journal of Biological Chemistry* 290(41):24705-24714.
59. Xiao S, *et al.* (2004) COS1: an Arabidopsis coronatine insensitive1 suppressor essential for regulation of jasmonate-mediated plant defense and senescence. *Plant Cell* 16(5):1132-1142.
60. Murguia, Belles J, & Serrano R (1995) A salt-sensitive 3'(2'),5'-bisphosphate nucleotidase involved in sulfate activation. *Science* 267(5195):232-234.

61. Hutchison RS & Ort DR (1995) [23] Measurement of equilibrium midpoint potentials of thiol/disulfide regulatory groups on thioredoxinactivated chloroplast enzymes. *Methods in Enzymology*, ed Lester P (Academic Press), Vol Volume 252, pp 220-228.
62. Karplus PA & Diederichs K (2012) Linking Crystallographic Model and Data Quality. *Science* 336(6084):1030-1033.
63. Diederichs K & Karplus PA (2013) Better models by discarding data? *Acta Crystallogr D Biol Crystallogr* 69(Pt 7):1215-1222.
64. Kabsch W (2010) Integration, scaling, space-group assignment and post-refinement. *Acta Crystallographica. Section D, Biological Crystallography* 66(Pt 2):133-144.
65. Winn MD, *et al.* (2011) Overview of the CCP4 suite and current developments. *Acta Crystallographica Section D* 67(4):235-242.
66. Adams PD, *et al.* (2010) PHENIX: a comprehensive Python-based system for macromolecular structure solution. *Acta Crystallographica Section D* 66(2):213-221.
67. McCoy AJ, *et al.* (2007) Phaser crystallographic software. *Journal of Applied Crystallography* 40(4):658-674.
68. Afonine PV, *et al.* (2012) Towards automated crystallographic structure refinement with phenix.refine. *Acta Crystallogr D Biol Crystallogr* 68(Pt 4):352-367.
69. Pronk S, *et al.* (2013) GROMACS 4.5: a high-throughput and highly parallel open source molecular simulation toolkit. *Bioinformatics (Oxford, England)* 29(7):845-854.
70. Schmid N, *et al.* (2011) Definition and testing of the GROMOS force-field versions 54A7 and 54B7. *Eur Biophys J* 40(7):843-856.
71. Berendsen HJC, Postma JPM, van Gunsteren WF, & Hermans J (1981) Interaction Models for Water in Relation to Protein Hydration. The Jerusalem Symposia on Quantum Chemistry and Biochemistry, ed Pullman B (Springer Netherlands), Vol 14, pp 331-342.
72. Essmann U, *et al.* (1995) A smooth particle mesh Ewald method. *The Journal of Chemical Physics* 103(19).
73. Lopez-Blanco JR, Garzon JI, & Chacon P (2011) iMod: multipurpose normal mode analysis in internal coordinates. *Bioinformatics* 27(20):2843-2850.
74. Ichiye T & Karplus M (1991) Collective motions in proteins: A covariance analysis of atomic fluctuations in molecular dynamics and normal mode simulations. *Proteins: Structure, Function, and Bioinformatics* 11(3):205-217.

Figure Legends

Fig. 1: *In vivo* AtSAL1 activity is down-regulated by oxidative stress.

(A) *In vivo* AtSAL1 activity is down-regulated by oxidative stress with negligible change in protein abundance (WW: Well-watered, MD: Mid-Drought, LD: Late-Drought, HL: High-light, MV: Methyl Viologen, H₂O₂: Hydrogen peroxide). Activity was measured without any reducing agent, while protein electrophoresis and western blotting were performed under reducing conditions for optimal protein transfer from gel to membrane. Similar results were obtained from two independent experiments. Means and standard error for three to four biological replicates per treatment are shown. a,b,c (p<0.05) show significant differences between treatments. (B) *In vivo* AtSAL1 activity is sensitive to redox state. Disrupting redox homeostasis at Photosystem I water-water cycle, ascorbate detoxification of ROS, cellular redox buffers or regeneration of oxidized proteins (also see Table S1) result in significantly greater (*: p<0.05, **: p<0.01) down-regulation of AtSAL1 activity compared to WT under high-light stress. Some mutants only show a trend of down-regulation in activity but the differences were not significant. Means and standard error for averaged relative activities of two biological replicates at three different concentrations of PAP per genotype are shown.

Fig. 2: Regulation of AtSAL1 activity by redox state *via* its intramolecular Cys167-Cys190 disulfide.

(A) Down-regulation of AtSAL1 activity by oxidation requires oxidation of cysteines, as mutagenesis of cysteines to alanine in AtSAL1 abrogated redox sensitivity. The redox sensitivity correlates with a band directly beneath the full length reduced protein (black arrow), which was determined to be a Cys167-Cys190 intramolecular disulfide (see Fig. 2C). Vertical dashed lines indicate splicing and truncation of the gel shown in full in Fig. 2C. Asterisk indicates p<0.1.

Activity of all proteins were assayed in the presence of 13.4 μ M PAP. Means and standard error of two independent experiments are shown. **(B)** Formation of disulfides in AtSAL1 by oxidation is rapidly reversed by returning the redox state to reducing conditions. Vertical dashed lines indicate splicing of the gel to show these three samples side-by-side; all samples were run on the same gel. **(C)** Determination of Cys-Cys disulfide pairs observed in WT AtSAL1 using cysteine to alanine substitution mutants of AtSAL1 under oxidation. Oxidized AtSAL1 proteins migrate at different rates to reduced AtSAL1 protein. The different Cys-Cys disulfide pairs were identified by cross-comparison to cysteine mutants: AtSAL1 containing a Cys167-Cys190 intramolecular disulfide (black triangles) migrates closest to reduced AtSAL1. The oxidized form is absent in all AtSAL1 mutants lacking either or both of Cys167 and Cys190. Other combinations such as the Cys21-Cys167 and Cys21-Cys190 disulfide did not correlate with the down-regulation of AtSAL1 activity by oxidation (Fig. 2A). These are likely non-specifically formed during protein denaturation and SDS-PAGE. AtSAL1 containing the Cys167-Cys190 intramolecular disulfide is the only oxidized AtSAL1 species detected in endogenous plant protein samples pretreated with iodoacetamide to block reduced cysteines during protein extraction to prevent non-specific disulfide formation (Fig. 6). Experiments were performed twice, with identical results.

Fig. 3: Structural basis for redox regulation of AtSAL1 activity.

(A) Structural elucidation of AtSAL1 reveals a dimerization interface, and three potentially redox-sensitive cysteine residues. Middle inset shows a view of the $2mFo-dFc$ map (blue lines, contoured at 1.0 σ) centered on Cys119 which is located at the interface between chain A (orange sticks) and chain B (green sticks), or a view of the $2mFo-dFc$ map centered on Cys167 and Cys190. Right inset shows the disulfide bonds present in an energy minimized model of the oxidized AtSAL1 dimer. **(B)** Closure of Loop 1 of AtSAL1, as predicted by normal mode

analysis (NMA). The lowest frequency normal mode is shown. Positions of C_α atoms are shown as coloured spheres, from the crystal structure (blue) to the most closed conformation (31). (C) Dimerization and disulfide formation reduces the mobility of key loops (loops 1, 3, 4, 8) in AtSAL1. Energy minimized models of the oxidized AtSAL1 dimer (left) or the reduced AtSAL1 monomer (middle) are colored according to mobility (blue least mobile to red most mobile) for details of energy minimization and normal mode analysis see methods. Right: plot of normal mode analysis (NMA) mobility by residue for the oxidized dimer and reduced monomer.

Fig. 4: AtSAL1 is also regulated via dimerization involving Cys119

(A) AtSAL1 in monomer-dimer equilibrium detected during size exclusion chromatography of purified recombinant protein. Dimers were detected in at least three independent purification runs. Inset: SDS-PAGE gel of monomeric and dimeric AtSAL1 indicating the proteins were of similar purity. The masses of the monomer and dimer were confirmed by SEC-MALLS (Fig. S1). (B) The monomer-dimer equilibrium can be shifted by an intermolecular disulfide under oxidizing conditions resulting in increased dimer abundance, or reduction of the disulfide by DTT dissociating the dimer. Whereas DTT is sufficient to achieve dimer separation, GSH is not. This is consistent with the relative redox potentials of these compounds: -264 mV at pH 7.4 for GSH compared to DTT (-360 mV) and the redox potential of disulfide bonds (ranging from -330 to -95 mV in thiol-disulfide oxidoreductases). Oxidation (DTT_{ox}, GSSG) increased dimer abundance to 100%, indicating formation of an intermolecular disulfide dimer under oxidation. Reversing the oxidation with reductant (DTT_{ox} + DTT and GSSG + DTT lanes) that breaks disulfide bonds shifts the equilibrium to monomer. The low resolution and fuzzy appearance of the higher MW bands are likely due to the type of gel (Tris-Glycine) as well as lack of detergent (SDS) and reductant (DTT) that inhibit resolving native, folded proteins that are also oxidized.

Similar results were obtained in two independent experiments. **(C)** Under redox titration by DTT_{ox} *in vitro*, which induces formation of the Cys167-Cys190 disulfide, only dimeric AtSAL1 showed significant down-regulation of activity. Identical results were obtained from two independent experiments. Inset: Dimerization is required for formation of the Cys167-Cys190 intramolecular disulfide that regulates AtSAL1 activity.

Fig. 5: AtSAL1 can be regulated by glutathionylation at redox-sensitive cysteines.

(A) Glutathionylation of AtSAL1 with oxidized glutathione (GSSG, yellow arrows) results in formation of the intramolecular C167-C190 disulfide (black arrows), presumably via the thiol-disulfide exchange mechanism (34). Identical results were obtained in two independent experiments. **(B)** *m/z* spectrum of AtSAL1 treated with GSSG and an untreated AtSAL1 sample, showing a shift in mass consistent with glutathionylation of the redox-sensitive Cys119 (red). Charge is indicated in brackets. In AtSAL1 treated with GSSG, glutathionylation was also detected on the Cys190 residue involved in intramolecular disulfide formation (not shown). **(C)** Both monomeric and dimeric AtSAL1 are sensitive to glutathionylation, with decrease in activity in redox titration with GSH/GSSG (a less negative redox potential indicates more oxidizing conditions). The redox midpoint potential (E_m) was close to physiological GSH/GSSG redox potential of Arabidopsis chloroplasts (35). Although activity of dimeric AtSAL1 is only decreased to 40% under fully oxidizing conditions compared to 10% for monomeric AtSAL1, the basal activity of dimeric AtSAL1 is already significantly lower than monomeric AtSAL1 under the same redox state (Table 1). Measurements were performed twice.

Fig. 6: AtSAL1 is redox-regulated *via* intramolecular disulfide formation and dimerization *in vivo*, and it is sensitive to the chloroplast redox state.

(A) Down-regulation of AtSAL1 activity and concomitant PAP accumulation correlates with formation of the Cys167-Cys190 intramolecular disulfide (black triangles) in endogenous AtSAL1 during drought stress. Means and standard error are shown for n=4 biological replicates for well-watered and n=3 for drought. In contrast to Fig. 1A, leaf protein extracts were blocked with iodoacetamide and then protein electrophoresis and western blotting were performed under non-reducing conditions to visualize the Cys167-Cys190 disulfide. Loading control was Coomassie Blue staining. Similar results were obtained in two independent experiments. (B) The monomer-dimer equilibrium of AtSAL1 in vivo is shifted in favor of the dimer during oxidative stress, suggesting formation of the Cys119-Cys119 intermolecular disulfide to stabilize the dimer. Total leaf protein pooled from four biological replicates per treatment was resolved on Native-PAGE, immunoblotted and the relative quantities of dimeric to monomeric AtSAL1 estimated by image analysis on ImageJ.

WW: Well-watered, MD: Mid-Drought, LD: Late-Drought, HL: High-light, MV: Methyl Viologen, H₂O₂: Hydrogen peroxide.

Fig.7: Biochemical and structural evidence for conservation of redox sensitivity in a rice SAL1 ortholog.

(A) Redox titration on OsSAL1 shows that the protein is redox sensitive and has a redox midpoint potentials (E_m) in the physiologically-relevant range. A less negative redox potential indicates more oxidizing conditions. (B) Oxidation of AtSAL1 and OsSAL1 with GSSG similarly result in glutathionylation of the proteins, increasing their apparent molecular weight when resolved on non-reducing SDS-PAGE (yellow triangles). Vertical dashed lines indicate splicing and truncation of the gel to remove additional lanes not relevant to this result. (C)

Comparison between redox-sensitive cysteine residues detected in structures of AtSAL1 and modelling of OsSAL1. Unlike AtSAL1 which contains both surface-exposed and intramolecular disulfide cysteines, OsSAL1 is predicted to contain surface exposed cysteines (marked in yellow). Both Cys203 and Cys221 of OsSAL1 are strongly conserved in *Poaceae* SAL1 orthologs (see Fig. S5).

Fig. 8: Enhancement of redox sensitivity in yeast ScHAL2 by introduction of the AtSAL1 intramolecular disulfide

(A) Structural alignment-guided introduction of the intramolecular disulfide from AtSAL1 (orange) into yeast ScHAL2 (gray) by the Tyr176Cys mutation. Thiol groups are indicated in yellow. (B) Introduction of additional disulfide in ScHAL2+3C results in increased redox sensitivity *in vitro* compared to WT ScHAL2. Means and standard error from two independent experiments for specific activity at 3.35 μ M PAP are shown. For full results, see Table S3. Asterisks indicate significant differences ($p < 0.05$). (C) Introduction of additional disulfide in ScHAL2+3C results in increased redox sensitivity and faster initiation of PAP accumulation *in vivo* when expressed in yeast *Ahal2* cells under mild oxidative stress. Significant differences are indicated by a,b ($p < 0.05$). Error bars indicate standard error; n=3 independent cultures for all experiments. n.s. = no significant difference

Fig. 1

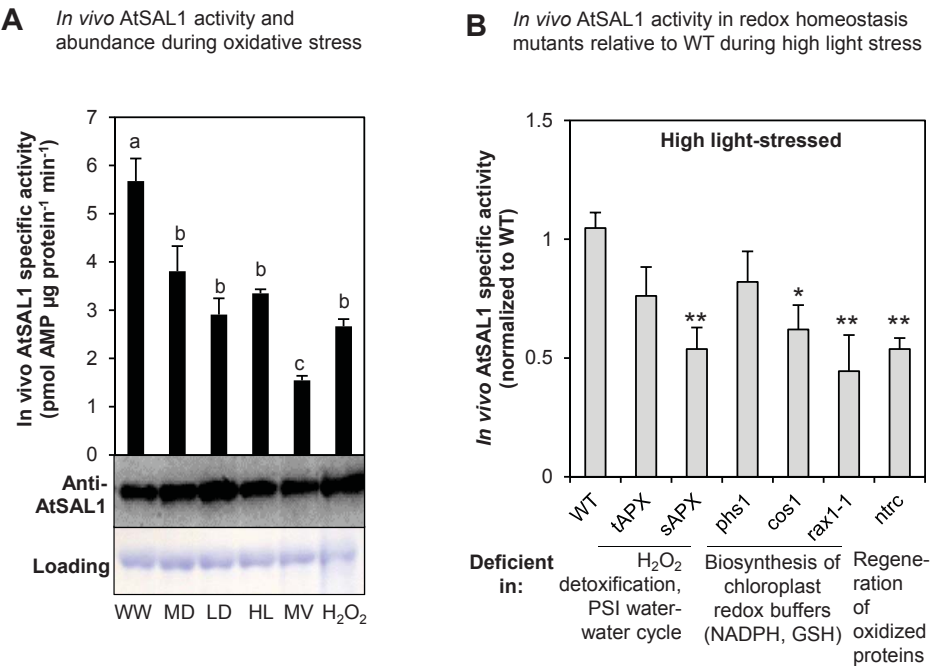
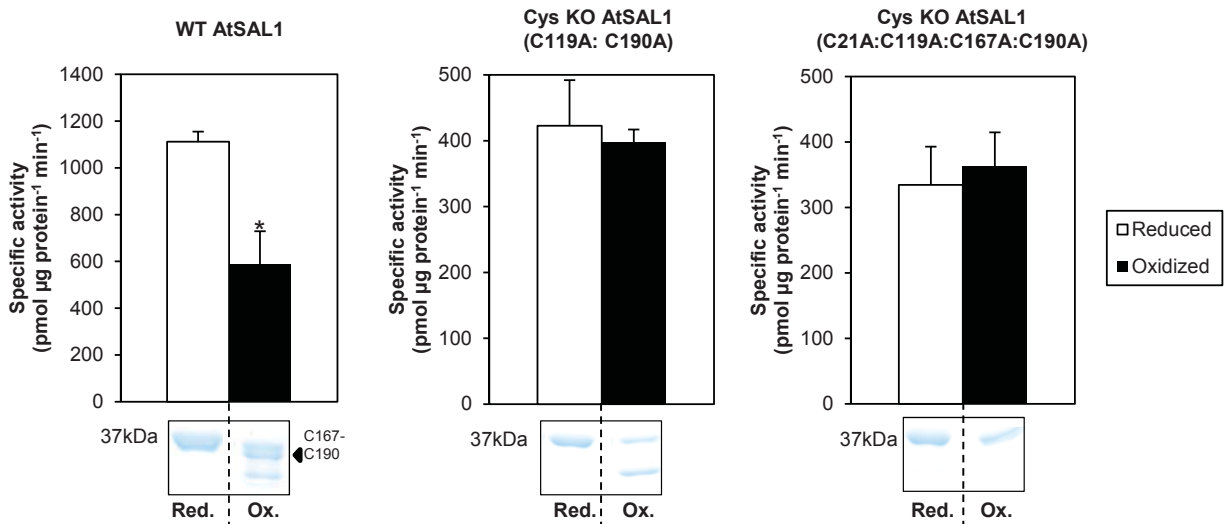


Fig. 1: *In vivo* AtSAL1 activity is down-regulated by oxidative stress.

(A) *In vivo* AtSAL1 activity is down-regulated by oxidative stress with negligible change in protein abundance (WW: Well-watered, MD: Mid-Drought, LD: Late-Drought, HL: High-light, MV: Methyl Viologen, H₂O₂: Hydrogen peroxide). Activity was measured without any reducing agent, while protein electrophoresis and western blotting were performed under reducing conditions for optimal protein transfer from gel to membrane. Similar results were obtained from two independent experiments. Means and standard error for three to four biological replicates per treatment are shown. a,b,c (p<0.05) show significant differences between treatments. (B) *In vivo* AtSAL1 activity is sensitive to redox state. Disrupting redox homeostasis at Photosystem I water-water cycle, ascorbate detoxification of ROS, cellular redox buffers or regeneration of oxidized proteins (also see Table S1) result in significantly greater (*: p<0.05, **: p<0.01) down-regulation of AtSAL1 activity compared to WT under high-light stress. Some mutants only show a trend of down-regulation in activity but the differences were not significant. Means and standard error for averaged relative activities of two biological replicates at three different concentrations of PAP per genotype are shown.

Fig. 2

A Dependence of AtSAL1 redox sensitivity on oxidation of cysteines and formation of a disulfide bond



B Reversibility of the disulfides in AtSAL1 by changes in redox state

Redox treatment	30 min oxidation (DTT _{ox})	30 min DTT
Reversibility treatment	-	1 min DTT
AtSAL1		

C Identification of the Cys167-Cys190 intramolecular disulfide in AtSAL1 *in vitro*

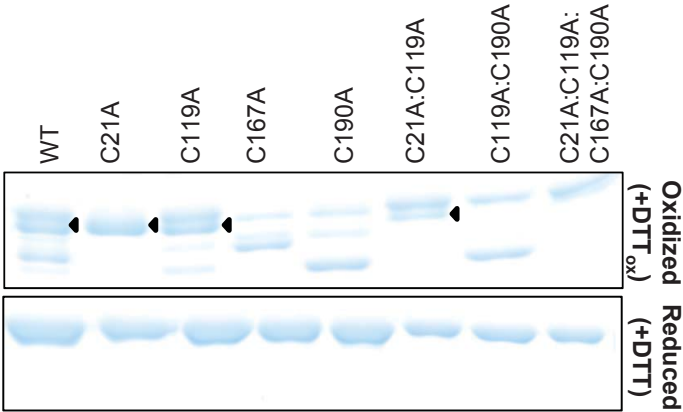
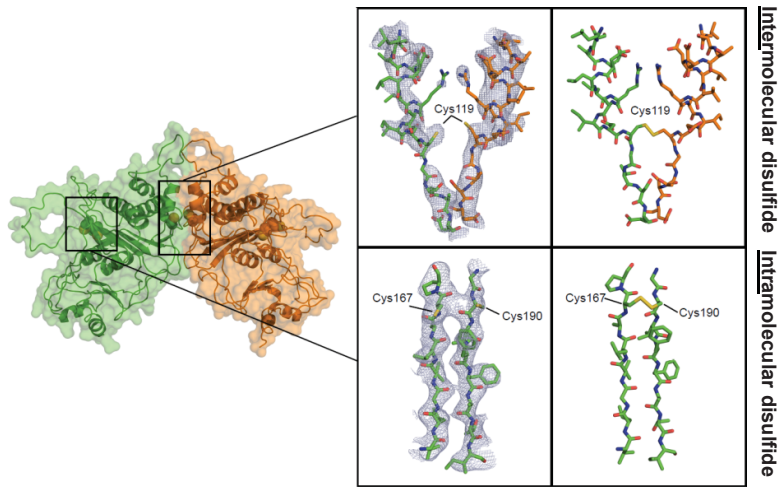


Fig. 2: Regulation of AtSAL1 activity by redox state via its intramolecular Cys167-Cys190 disulfide.

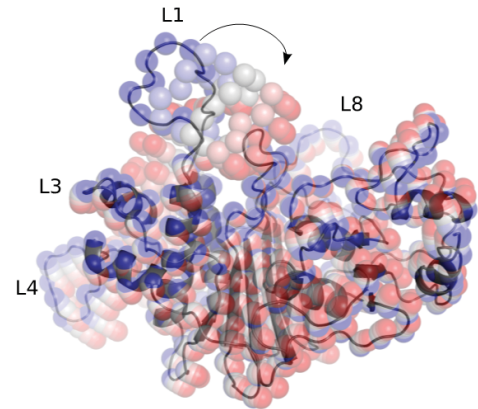
(A) Down-regulation of AtSAL1 activity by oxidation requires oxidation of cysteines, as mutagenesis of cysteines to alanine in AtSAL1 abrogated redox sensitivity. The redox sensitivity correlates with a band directly beneath the full length reduced protein (black arrow), which was determined to be a Cys167-Cys190 intramolecular disulfide (see Fig. 2C). Vertical dashed lines indicate splicing and truncation of the gel shown in full in Fig. 2C. Asterisk indicates $p < 0.1$. Activity of all proteins were assayed in the presence of $13.4 \mu\text{M}$ PAP. Means and standard error of two independent experiments are shown. **(B)** Formation of disulfides in AtSAL1 by oxidation is rapidly reversed by returning the redox state to reducing conditions. Vertical dashed lines indicate splicing of the gel to show these three samples side-by-side; all samples were run on the same gel. **(C)** Determination of Cys-Cys disulfide pairs observed in WT AtSAL1 using cysteine to alanine substitution mutants of AtSAL1 under oxidation. Oxidized AtSAL1 proteins migrate at different rates to reduced AtSAL1 protein. The different Cys-Cys disulfide pairs were identified by cross-comparison to cysteine mutants: AtSAL1 containing a Cys167-Cys190 intramolecular disulfide (black triangles) migrates closest to reduced AtSAL1. The oxidized form is absent in all AtSAL1 mutants lacking either or both of Cys167 and Cys190. Other combinations such as the Cys21-Cys167 and Cys21-Cys190 disulfide did not correlate with the down-regulation of AtSAL1 activity by oxidation (Fig. 2A). These are likely non-specifically formed during protein denaturation and SDS-PAGE. AtSAL1 containing the Cys167-Cys190 intramolecular disulfide is the only oxidized AtSAL1 species detected in endogenous plant protein samples pretreated with iodoacetamide to block reduced cysteines during protein extraction to prevent non-specific disulfide formation (Fig. 6). Experiments were performed twice, with identical results.

Fig. 3

A Protein structure of AtSAL1 with potential intermolecular and intramolecular disulfides



B Closure of loop 1 in AtSAL1



C Effect of dimerization and disulfide bonding on flexibility of AtSAL1 protein loops

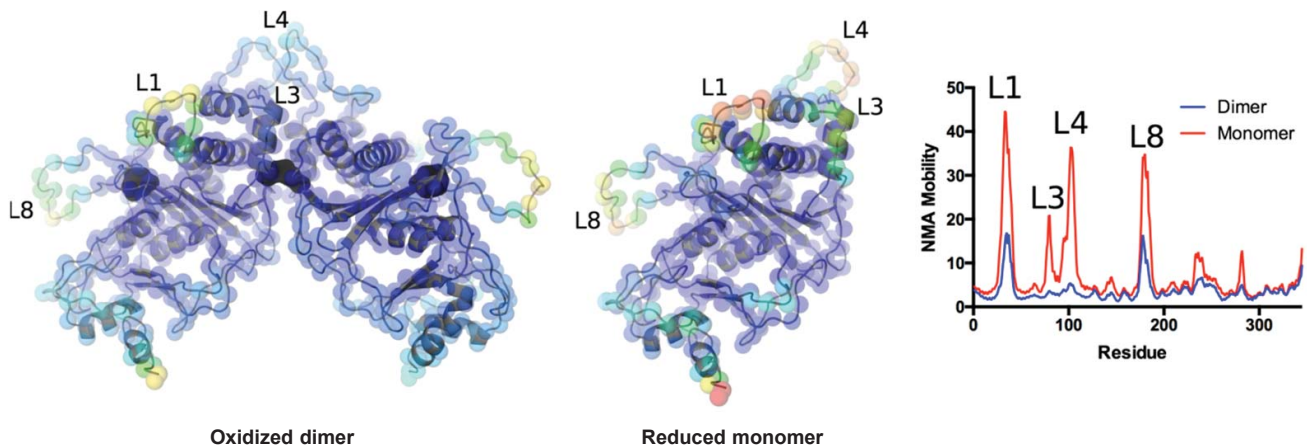
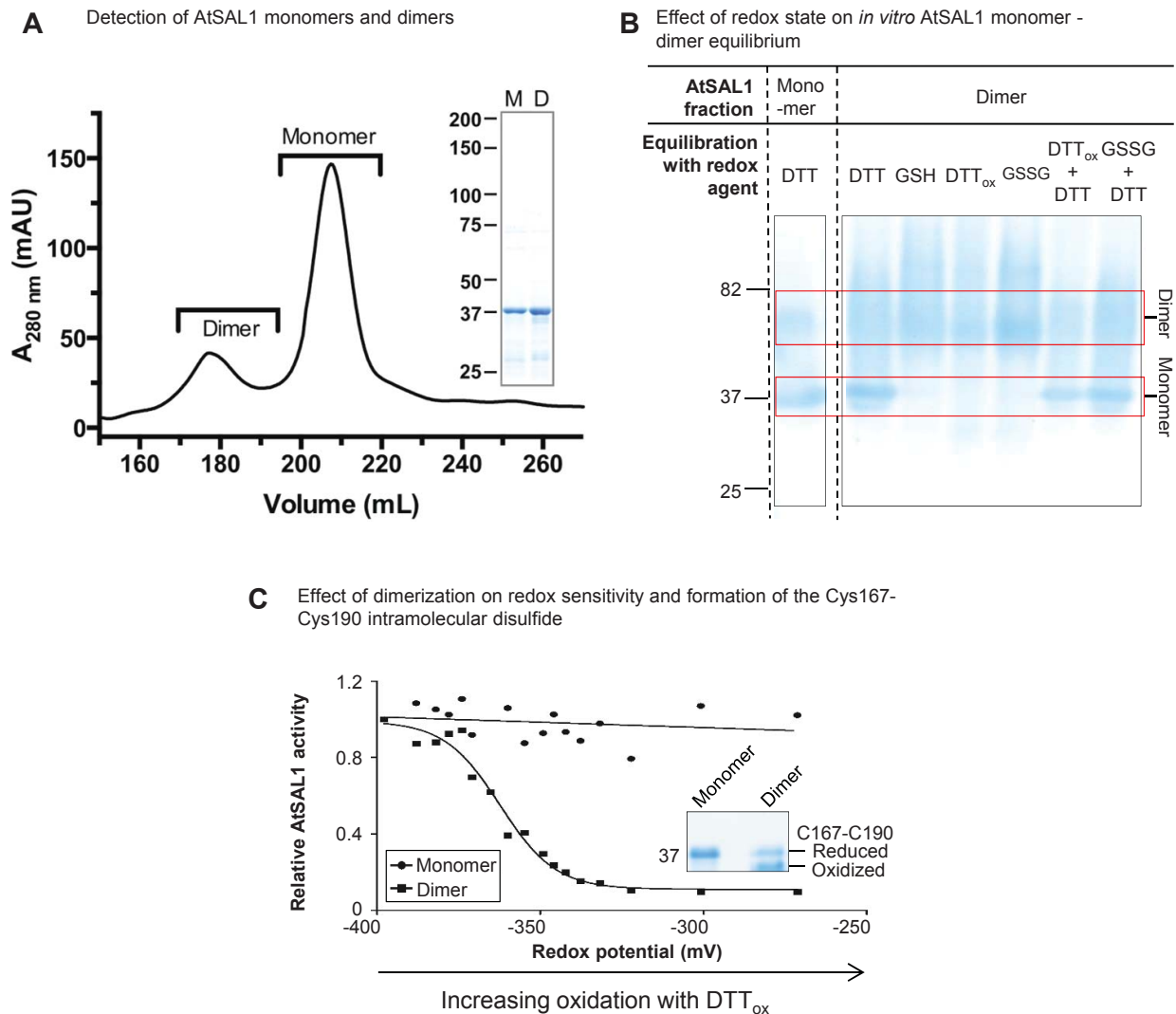
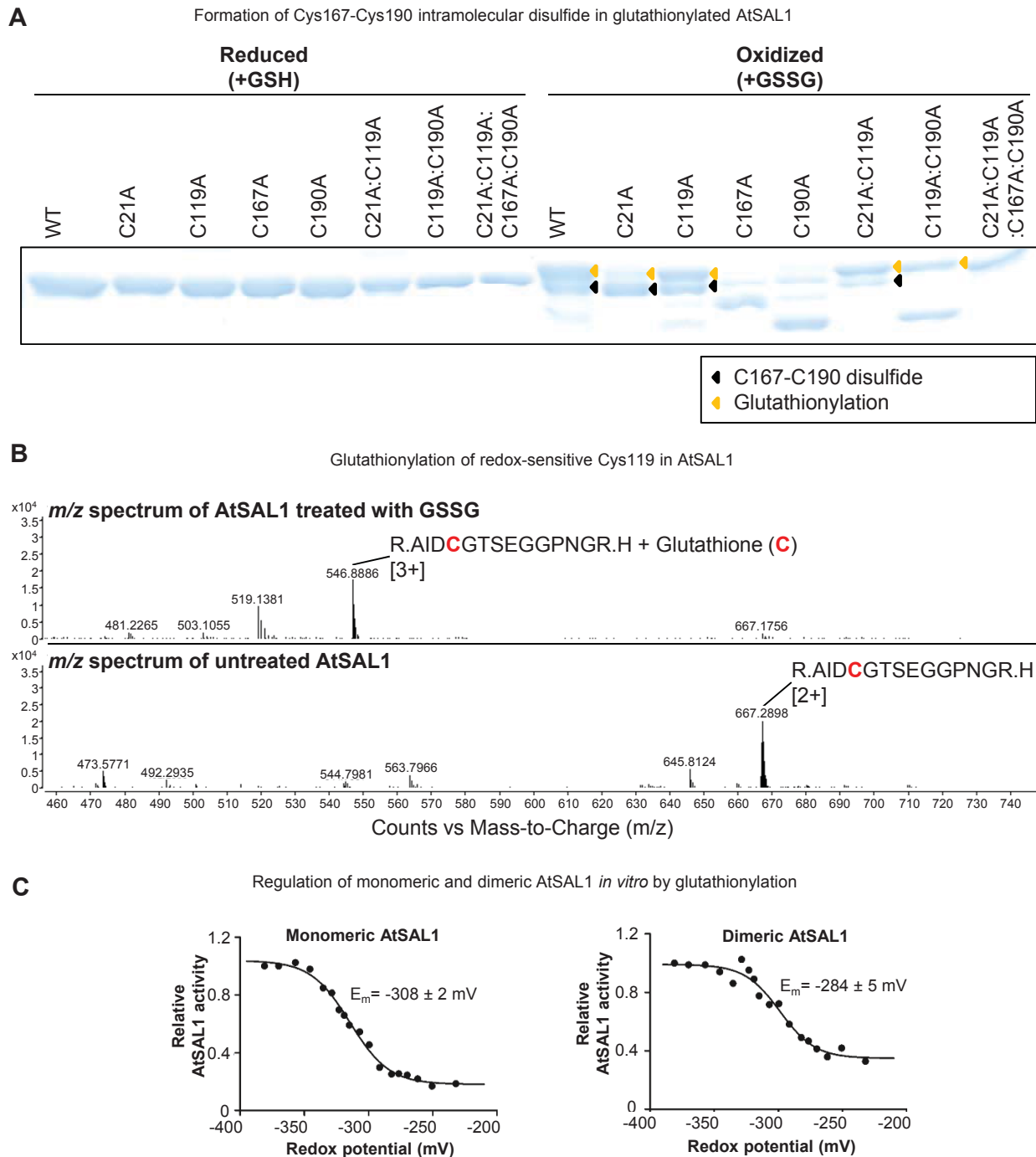


Fig. 3: Structural basis for redox regulation of AtSAL1 activity.

(A) Structural elucidation of AtSAL1 reveals a dimerization interface, and three potentially redox-sensitive cysteine residues. Middle inset shows a view of the $2mFo-dFc$ map (blue lines, contoured at 1.0σ) centered on Cys119 which is located at the interface between chain A (orange sticks) and chain B (green sticks), or a view of the $2mFo-dFc$ map centered on Cys167 and Cys190. Right inset shows the disulfide bonds present in an energy minimized model of the oxidized AtSAL1 dimer. **(B)** Closure of Loop 1 of AtSAL1, as predicted by normal mode analysis (NMA). The lowest frequency normal mode is shown. Positions of C_{α} atoms are shown as coloured spheres, from the crystal structure (blue) to the most closed conformation (31). **(C)** Dimerization and disulfide formation reduces the mobility of key loops (loops 1, 3, 4, 8) in AtSAL1. Energy minimized models of the oxidized AtSAL1 dimer (left) or the reduced AtSAL1 monomer (middle) are colored according to mobility (blue least mobile to red most mobile) for details of energy minimization and normal mode analysis see methods. Right: plot of normal mode analysis (NMA) mobility by residue for the oxidized dimer and reduced monomer.

Fig. 4**Fig. 4: AtSAL1 is also regulated via dimerization involving Cys119**

(A) AtSAL1 in monomer-dimer equilibrium detected during size exclusion chromatography of purified recombinant protein. Dimers were detected in at least three independent purification runs. Inset: SDS-PAGE gel of monomeric and dimeric AtSAL1 indicating the proteins were of similar purity. The masses of the monomer and dimer were confirmed by SEC-MALLS (Fig. S1). (B) The monomer-dimer equilibrium can be shifted by an intermolecular disulfide under oxidizing conditions resulting in increased dimer abundance, or reduction of the disulfide by DTT dissociating the dimer. Whereas DTT is sufficient to achieve dimer separation, GSH is not. This is consistent with the relative redox potentials of these compounds: -264 mV at pH 7.4 for GSH compared to DTT (-360 mV) and the redox potential of disulfide bonds (ranging from -330 to -95 mV in thiol-disulfide oxidoreductases). Oxidation (DTT_{ox}, GSSG) increased dimer abundance to 100%, indicating formation of an intermolecular disulfide dimer under oxidation. Reversing the oxidation with reductant (DTT_{ox} + DTT and GSSG + DTT lanes) that breaks disulfide bonds shifts the equilibrium to monomer. The low resolution and fuzzy appearance of the higher MW bands are likely due to the type of gel (Tris-Glycine) as well as lack of detergent (SDS) and reductant (DTT) that inhibit resolving native, folded proteins that are also oxidized. Similar results were obtained in two independent experiments. (C) Under redox titration by DTT_{ox} *in vitro*, which induces formation of the Cys167-Cys190 disulfide, only dimeric AtSAL1 showed significant down-regulation of activity. Identical results were obtained from two independent experiments. Inset: Dimerization is required for formation of the Cys167-Cys190 intramolecular disulfide that regulates AtSAL1 activity.

Fig. 5**Fig. 5: AtSAL1 can be regulated by glutathionylation at redox-sensitive cysteines.**

(A) Glutathionylation of AtSAL1 with oxidized glutathione (GSSG, yellow arrows) results in formation of the intramolecular C167-C190 disulfide (black arrows), presumably via the thiol-disulfide exchange mechanism (34). Identical results were obtained in two independent experiments. **(B)** *m/z* spectrum of AtSAL1 treated with GSSG and an untreated AtSAL1 sample, showing a shift in mass consistent with glutathionylation of the redox-sensitive Cys119 (red). Charge is indicated in brackets. In AtSAL1 treated with GSSG, glutathionylation was also detected on the Cys190 residue involved in intramolecular disulfide formation (not shown). **(C)** Both monomeric and dimeric AtSAL1 are sensitive to glutathionylation, with decrease in activity in redox titration with GSH/GSSG (a less negative redox potential indicates more oxidizing conditions). The redox midpoint potential (E_m) was close to physiological GSH/GSSG redox potential of Arabidopsis chloroplasts (35). While dimeric AtSAL1 activity was only decreased to 40% under fully oxidizing conditions compared to 10% for monomeric AtSAL1, the basal activity of dimeric AtSAL1 was already significantly lower than monomeric AtSAL1 under the same redox state (Table 1). Measurements were performed twice.

Fig. 6

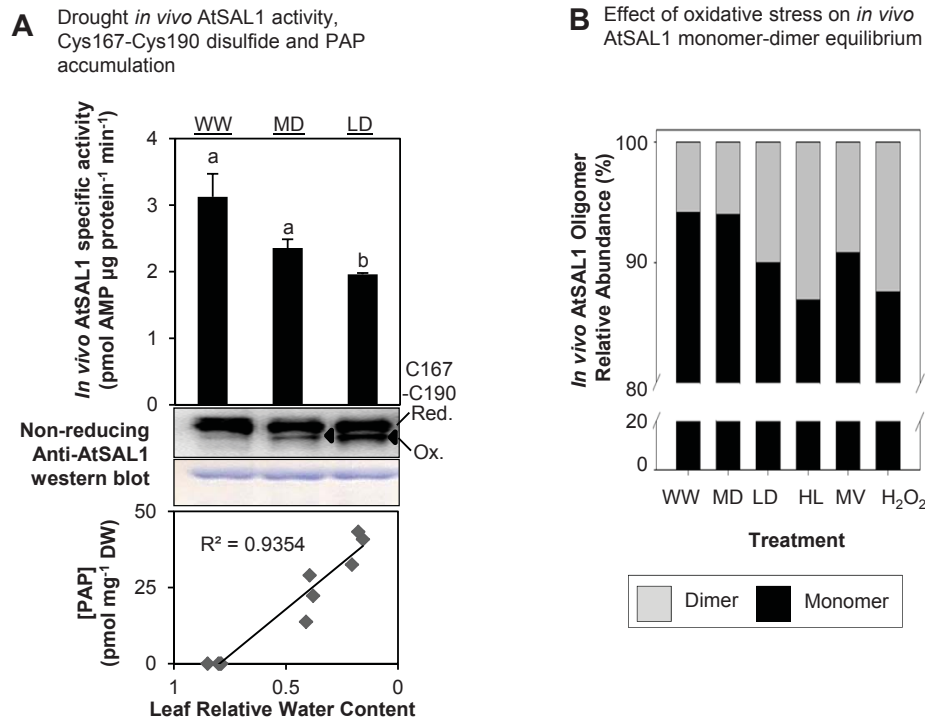


Fig. 6: AtSAL1 is redox-regulated via intramolecular disulfide formation and dimerization *in vivo*, and it is sensitive to the chloroplast redox state.

(A) Down-regulation of AtSAL1 activity and concomitant PAP accumulation correlates with formation of the Cys167-Cys190 intramolecular disulfide (black triangles) in endogenous AtSAL1 during drought stress. Means and standard error are shown for n=4 biological replicates for well-watered and n=3 for drought. In contrast to Fig. 1A, leaf protein extracts were blocked with iodoacetamide and then protein electrophoresis and western blotting were performed under non-reducing conditions to visualize the Cys167-Cys190 disulfide. Loading control was Coomassie Blue staining. Similar results were obtained in two independent experiments. **(B)** The monomer-dimer equilibrium of AtSAL1 *in vivo* is shifted in favor of the dimer during oxidative stress, suggesting formation of the Cys119-Cys119 intermolecular disulfide to stabilize the dimer. Total leaf protein pooled from four biological replicates per treatment was resolved on Native-PAGE, immunoblotted and the relative quantities of dimeric to monomeric AtSAL1 estimated by image analysis on ImageJ.

WW: Well-watered, MD: Mid-Drought, LD: Late-Drought, HL: High-light, MV: Methyl Viologen, H₂O₂: Hydrogen peroxide.

Fig. 7

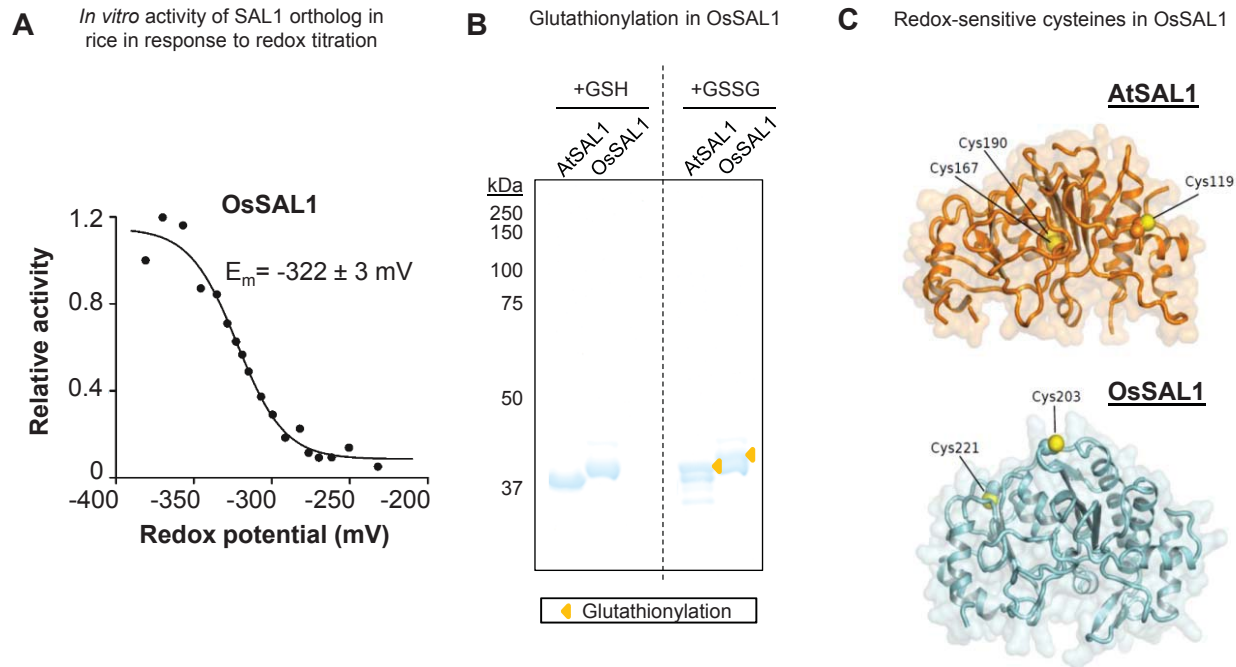


Fig.7: Biochemical and structural evidence for conservation of redox sensitivity in a rice SAL1 ortholog.

(A) Redox titration on OsSAL1 shows that the protein is redox sensitive and has a redox midpoint potentials (E_m) in the physiologically-relevant range. A less negative redox potential indicates more oxidizing conditions. **(B)** Oxidation of AtSAL1 and OsSAL1 with GSSG similarly result in glutathionylation of the proteins, increasing their apparent molecular weight when resolved on non-reducing SDS-PAGE (yellow triangles). Vertical dashed lines indicate splicing and truncation of the gel to remove additional lanes not relevant to this result. **(C)** Comparison between redox-sensitive cysteine residues detected in structures of AtSAL1 and modelling of OsSAL1. Unlike AtSAL1 which contains both surface-exposed and intramolecular disulfide cysteines, OsSAL1 is predicted to contain surface exposed cysteines (marked in yellow). Both Cys203 and Cys221 of OsSAL1 are strongly conserved in *Poaceae* SAL1 orthologs (see Fig. S5).

Fig. 8

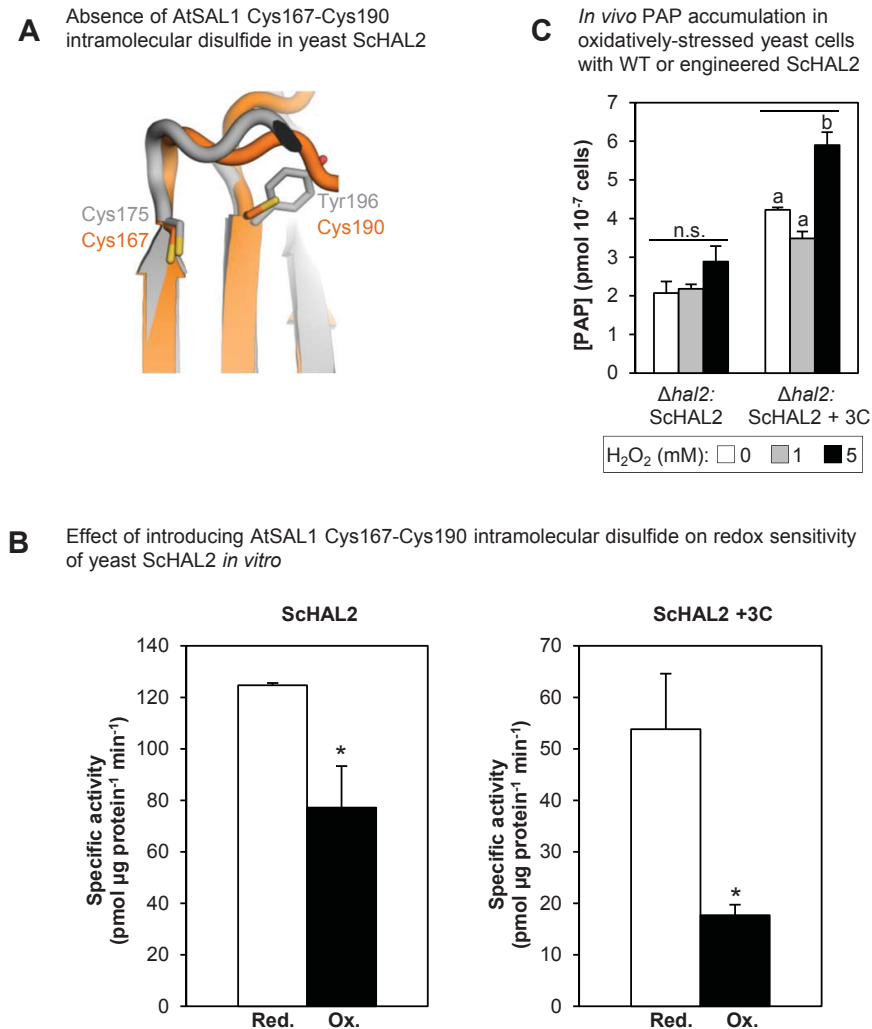


Fig. 8: Enhancement of redox sensitivity in yeast SchAL2 by introduction of the AtSAL1 intramolecular disulfide
(A) Structural alignment-guided introduction of the intramolecular disulfide from AtSAL1 (orange) into yeast SchAL2 (gray) by the Tyr176Cys mutation. Thiol groups are indicated in yellow. **(B)** Introduction of additional disulfide in SchAL2+3C results in increased redox sensitivity *in vitro* compared to WT SchAL2. Means and standard error from two independent experiments for specific activity at 3.35 μM PAP are shown. For full results, see Table S3. Asterisks indicate significant differences ($p < 0.05$). **(C)** Introduction of additional disulfide in SchAL2+3C results in increased redox sensitivity and faster initiation of PAP accumulation *in vivo* when expressed in yeast $\Delta hal2$ cells under mild oxidative stress. Significant differences are indicated by a,b ($p < 0.05$). Error bars indicate standard error; $n=3$ independent cultures for all experiments. n.s. = no significant difference

Table 1

Kinetic parameters	Monomeric AtSAL1		Dimeric AtSAL1	
	Reduced	Oxidized	Reduced	Oxidized
K_M (μM PAP)	9.9 ± 3.3	8.3 ± 1.2	8.7 ± 5.2	4.2 ± 1.8
k_{cat} (min^{-1})	123 ± 18	119 ± 13	24.4 ± 1.1	4.3 ± 1.3
k_{cat} / K_M ($\mu\text{M}^{-1} \text{min}^{-1}$)	12.4	14.2	2.8	1.0

Table 1: Effect of dimerization on redox sensitivity and enzyme kinetics of AtSAL1 under different redox states.

All enzymatic assays were performed with 0.2 μg recombinant protein in the presence of 5mM DTT (reduced) or DTT_{ox} (oxidized) at 25°C. Results shown are means and standard error from two independent experiments.

Table 2

Kinetic parameters	OsSAL1	
	Reduced	Oxidized
K_M (μM PAP)	20 ± 6.9	61 ± 23.6
k_{cat} (min^{-1})	44 ± 3.9	11 ± 1.5
k_{cat} / K_M ($\mu\text{M}^{-1} \text{min}^{-1}$)	2.2	0.2

Table 2: Effect of oxidation on enzyme kinetics of the riceSAL1 ortholog, OsSAL1.

Enzymatic assays were performed with 0.2 μg recombinant protein in the presence of 20mM GSH (reduced) or GSSG (oxidized) at 25°C. Experiment was performed twice, with similar results.

Fig. S1

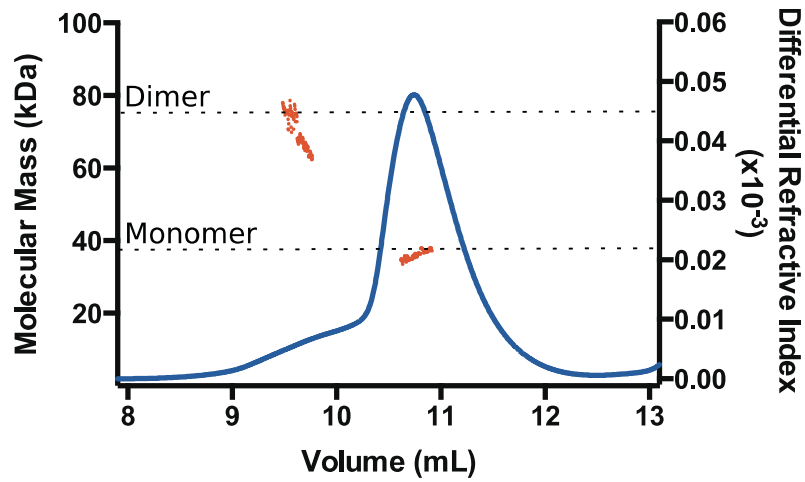


Fig. S1: AtSAL1 exists in a monomer-dimer equilibrium.

Purified AtSAL1 was exchanged into assay buffer and analysed by MALLS following separation by size exclusion chromatography. Differential refractive index is shown as a blue line (right axis) and molecular mass derived from light scattering data as shown as red points (left axis). The expected masses of AtSAL1 monomer (37.5 kDa) and dimer (75 kDa) are indicated by dashed lines.

Fig. S2

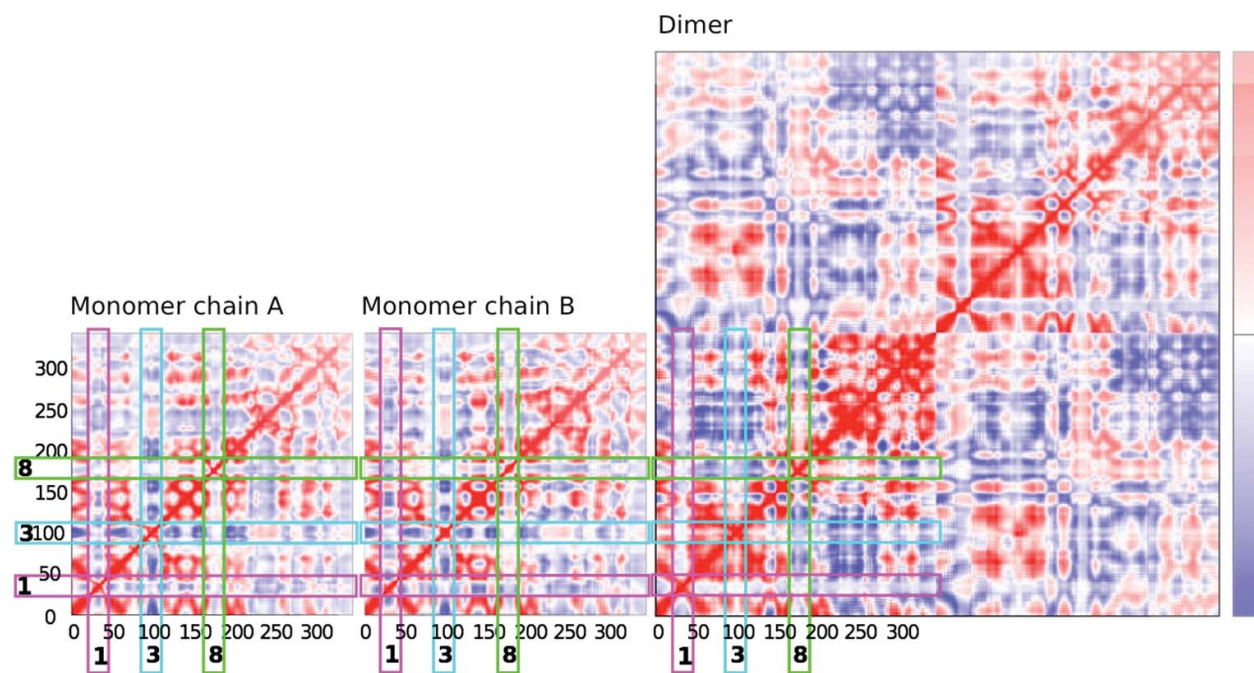


Fig. S2: Prediction of coupled motions in AtSAL1.

Covariance maps of C_{α} motions (74) calculated for the reduced AtSAL1 monomer and oxidized AtSAL1 dimer. Residues with coupled motions are shown in red, residues with anti-correlated motions are shown in blue. The positions of the mobile loops described in Fig. 3C (loops 1,3,8) are indicated.

Fig. S3

Formation of intramolecular disulfide *via* glutathionylation and thiol-disulfide exchange

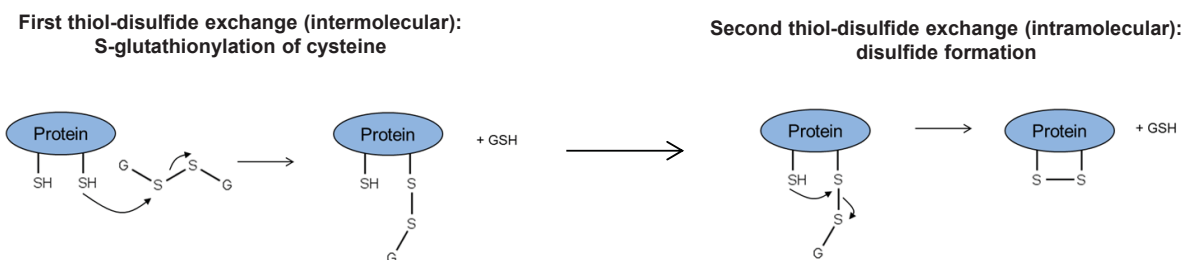


Fig. S3: Formation of an intramolecular disulfide via a thiol-disulfide exchange initiated by glutathionylation of a cysteine residue. See ref 34 for review of this mechanism.

Fig. S4

Effect of substituting redox-sensitive cysteines in AtSAL1 on protein stability and abundance in the soluble fraction when heterologously expressed in *E. coli*

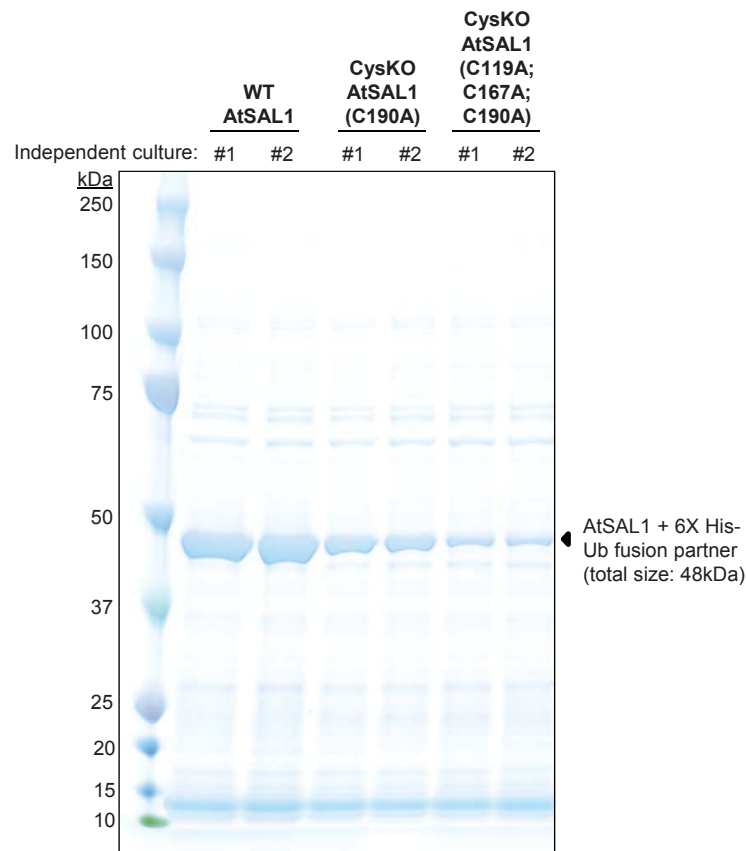


Fig. S4: Cys-Ala mutations negatively affect AtSAL1 protein stability and abundance. The yield of soluble AtSAL1 protein is drastically decreased when the redox-sensitive Cys residues were mutagenized to Ala. The SDS-PAGE gel shows semi-purified recombinant WT or mutated AtSAL1 proteins after a soluble protein fraction from 7 mL of induced *E. coli* cells was incubated with Ni-NTA beads in a 1.5mL Eppendorf tube, washed with 20mM imidazole, and the bound AtSAL1 + 6X His-Ub fusion proteins (black triangles) eluted with 250mM imidazole. The abundance of soluble AtSAL1 protein decreased with increasing number of Cys-Ala substitutions. The negative effect of the Cys-Ala mutations was reproducible in 2 independent transformed bacterial colonies.

Fig. S5

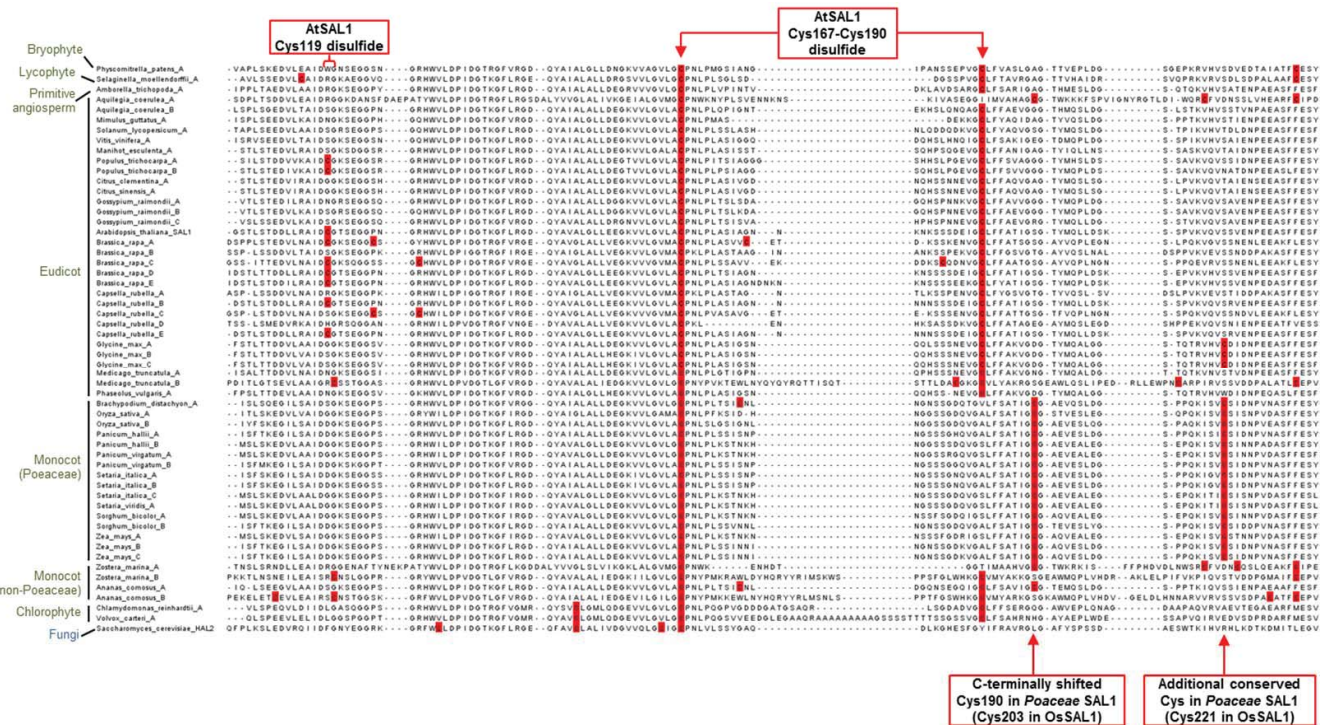


Fig. S5: Conservation of redox-sensitive cysteines in SAL1 orthologs in plants. The Cys119 involved in dimerization of AtSAL1 is moderately conserved in eudicots and non-*Poaceae* monocot plants, but is absent in other lineages. The intramolecular disulfide pair Cys167-Cys190 is invariant across bryophytes, lycophytes, primitive angiosperm, eudicots and non-*Poaceae* monocots. Cys190 is C-terminally shifted by seven amino acids in *Poaceae* monocot plants. Additionally, another cysteine is strongly conserved in the *Poaceae* family of monocots (Cys221 in OsSAL1; see Fig. 7). In contrast to plant SAL1 orthologs (green), the fungal SAL1 ortholog in *Saccharomyces cerevisiae* HAL2 (blue) lacks Cys119 and Cys190.

Fig. S6

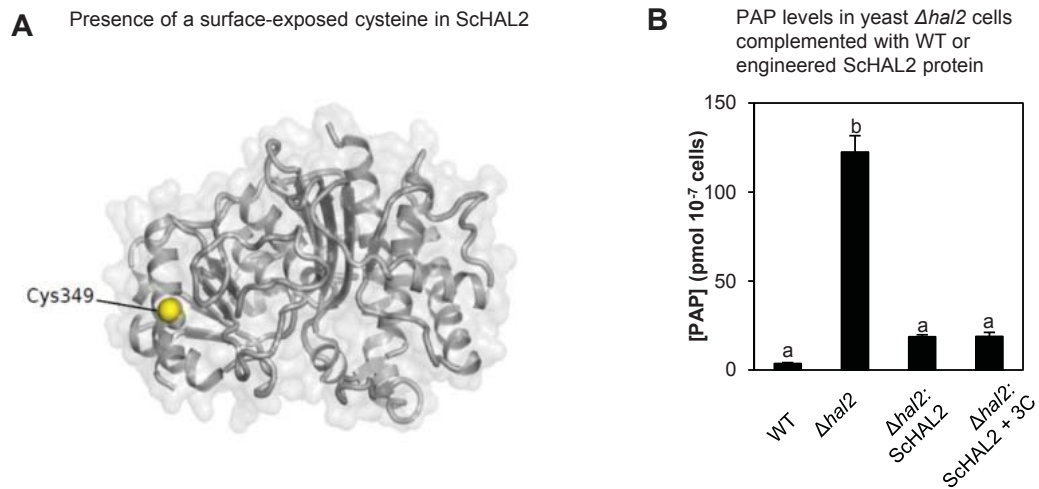


Fig. S6: WT and engineered SchAL2. (A) Presence of a surface-exposed Cys349 in the SchAL2 crystal structure (1KA1), which may explain the redox sensitive activity observed in Fig. 8B. (B) The WT SchAL2 and SchAL2+3C proteins are equally active *in vivo* when expressed in yeast cells deficient in SchAL2 ($\Delta hal2$), as both proteins complement PAP levels in $\Delta hal2$ to similar levels, albeit still about 10-fold higher than WT. Similar results were obtained in two independent experiments.

Table S1

Name	Gene Identifier	Type of mutation	Biological pathway affected	Ref.
<i>tAPX</i> (thylakoidal Ascorbate Peroxidase)	AT1G77490	amiRNA-knockdown	Detoxification of H ₂ O ₂ in the chloroplast thylakoid, detoxification of superoxide by superoxide dismutase in water-water cycle at Photosystem I (PSI).	1
<i>sAPX</i> (stromal Ascorbate Peroxidase)	AT4G08390	T-DNA insertion, homozygous	Detoxification of H ₂ O ₂ in the chloroplast stroma, where AtSAL1 is also located	1
<i>phs1</i> (photosensitive 1)	AT3G47390	T-DNA insertion, homozygous	Involved in riboflavin and FAD synthesis. Mutant allele has increased oxidative stress due to reduced NADPH/NADP ⁺ ratios and overproduction of ROS at PSI under high light.	53
<i>cos1</i> (coronatine insensitive1 suppresor)	AT2G44050	T-DNA insertion, heterozygous	Involved in the same metabolic pathway as <i>phs1</i> (riboflavin and FAD synthesis).	59
<i>rax1-1</i> (regulator of Ascorbate Peroxidase 2 1-1)	AT4G23100	Point mutation, homozygous	Rate-limiting step of glutathione synthesis. GSH:GSSG redox ratio may be altered under oxidative stress.	54
<i>ntrc</i> (NAPDH-dependent Thioredoxin Reductase C)	AT2G41680	T-DNA insertion, homozygous	Reduction of 2-Cys peroxiredoxins and redox control within the chloroplast. Deficiency causes hypersensitivity to abiotic stress	52

Table S1: Summary of redox homeostasis-deficient mutants used in Fig. 1.

Loss-of-function mutants deficient in various aspects of redox homeostasis in the chloroplast were chosen for analysis of AtSAL1 activity under abiotic stress. The mutants are deficient in ROS detoxification, redox control at PSI, or chloroplast redox buffer pathways.

Table S2

Table S2: Data collection and refinement statistics for crystal structure of AtSAL1

AtSAL1 (PDB 5ESY)	
Data Processing	
Space group	$P6_1$
Cell dimensions (Å) a,b,c	137.14 137.14 74.64
α, β, γ (°)	90, 90, 120
Resolution range (Å)	38.247 - 3.05 (3.24 -3.05) ¹
Total number of reflections	125243 (20978)
Number of unique reflections	15341 (2522)
Multiplicity	8.2 (8.3)
Completeness (%)	99.63 (92.8)
Mean I/ σ (I)	15.23 (2.2)
Wilson B factor (Å ²)	83.6
² CC _{1/2}	0.999 (0.620)
R _{merge}	0.1042 (1.110)
Refinement	
R _{work} /R _{free}	0.220/ 0.264 (0.324/0.409)
Total number of atoms	5095
Protein	5095
Ligand/ion	0
Water	0
RMSD for bonds (Å)	0.011
RMSD for angles (deg)	1.47
Ramachandran favored (%)	87
Ramachandran outliers (%)	3
Clashscore	13
Average B factor (Å ²)	106.0

¹ Values in parenthesis are for the highest resolution shell.

² Pearson's correlation coefficient calculated from two half-sets of the data (63, 64).

Table S3

Protein	[PAP] (μM)	Specific Activity ($\text{pmol } \mu\text{g prot}^{-1} \text{ min}^{-1}$)		Decrease in Activity (%)	
		Reduced	Oxidized		Average
ScHAL2	3.35	124 ± 0.9	77 ± 16	38	
	13.4	414 ± 66	220 ± 31	46	46 ± 4.8^a
	26.8	597 ± 150	270 ± 35	54	
ScHAL2+3C	3.35	53 ± 10	17 ± 2	67	67 ± 1.4^b ($p < 0.005$ relative to ScHAL2)
	13.4	72 ± 24	25 ± 5	65	
	26.8	81 ± 29	24 ± 0.8	70	

Table S3: Effect of introducing AtSAL1 Cys167-Cys190 disulfide pair on redox sensitivity of ScHAL2.

Enzymatic assays were performed with 0.2 μg recombinant protein in the presence of 20mM GSH (reduced) or GSSG (oxidized) at 30°C. Means and standard error from two independent experiments are shown. The decrease in activity for ScHAL2+3C by oxidation is significantly greater (a,b; $p < 0.005$) than that in WT ScHAL2.